

Genetic dissection of MutL complexes in *Arabidopsis* meiosis

Nadia Kbir¹, Nadia Fernández-Jiménez², Wojciech Dziegielewski¹,
Esperanza Sáez-Zárate¹, Alexandre Pelé¹, Ana Mata-Villanueva^{2,3}, Julia Dluzewska¹,
Juan L. Santos², Mónica Pradillo^{2,*}, Piotr A. Ziolkowski^{1,*}

¹Laboratory of Genome Biology, Institute of Molecular Biology and Biotechnology, Adam Mickiewicz University, 61-614 Poznan, Poland

²Departamento de Genética, Fisiología y Microbiología, Facultad de Ciencias Biológicas, Universidad Complutense de Madrid, 28040 Madrid, Spain

³Present address: Centro de Biología Molecular Severo Ochoa, CSIC-UAM, Cantoblanco, 28049 Madrid, Spain

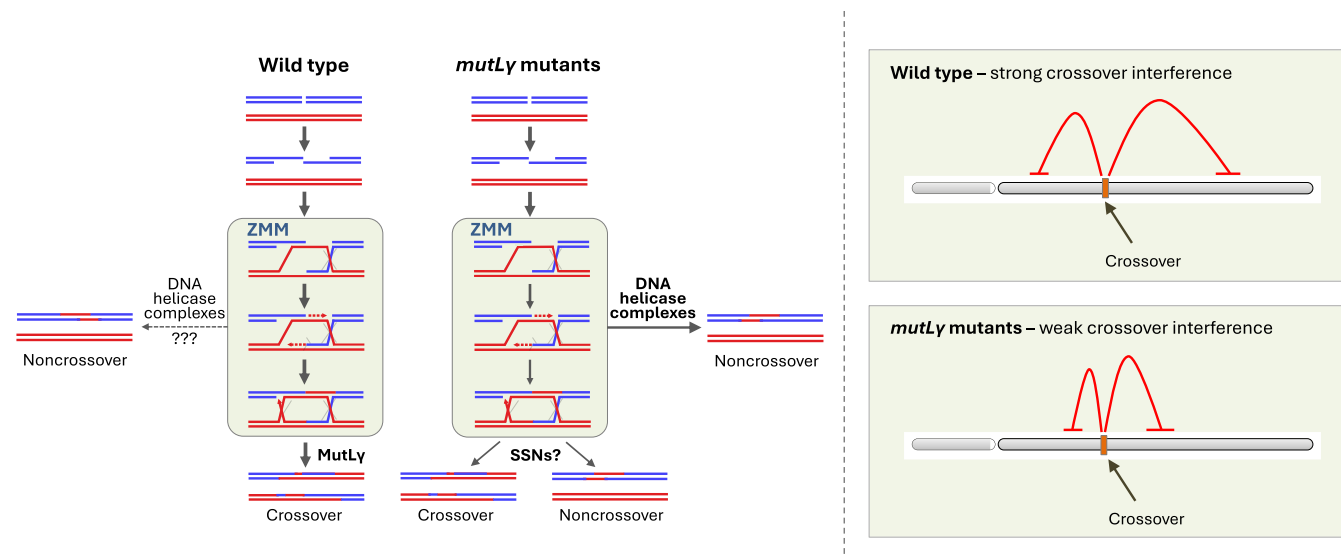
*To whom correspondence should be addressed. Email: pzio@amu.edu.pl

Correspondence may also be addressed to Mónica Pradillo. Email: pradillo@bio.ucm.es

Abstract

During meiosis, homologous chromosomes exchange genetic material through crossing over. The main crossover pathway relies on ZMM proteins, including ZIP4 and HEI10, and is typically resolved by the MLH1/MLH3 heterodimer, MutL γ . Our analysis shows that while MUS81 may partially compensate for MutL γ loss, its role remains uncertain. However, our multiple mutant analysis shows that MUS81 is unlikely to be the sole resolvase of ZMM-protected recombination intermediates when MutL γ is absent. Comparing genome-wide crossover maps of *mlh1* mutants with ZMM-deficient mutants and lines with varying HEI10 levels reveals that crossover interference persists in *mlh1* but is weakened. The significant crossover reduction in *mlh1* also increases aneuploidy in offspring. The loss of MutL γ can be suppressed by eliminating the FANCM helicase. Combined with the lower-than-expected chiasma frequency, this suggests that in MutL γ absence, some ZMM-protected intermediates are ultimately resolved by DNA helicases and/or their complexes with Top3 α . Elevated *MLH1* or *MLH3* expression moderately increases crossover frequency, while their misregulation drastically reduces crossover numbers and plant fertility, highlighting the importance for tight control of MLH1/MLH3 levels. By contrast, PMS1, a component of the MutL α endonuclease, appears uninvolved in crossing over. Together, these findings demonstrate the unique role of MutL γ in ZMM-dependent crossover regulation.

Graphical abstract



Introduction

Meiosis is a reductive cell division that results in the formation of gametes or spores, thereby enabling sexual reproduction [1]. It plays a vital role in generating genetic diversity within

populations [2]. Several mechanisms operate during meiosis to foster the creation of new genetic variations. One such mechanism is crossover recombination, where fragments are reciprocally exchanged between homologous chromosomes [3–5].

Received: October 1, 2024. Revised: February 16, 2025. Editorial Decision: February 20, 2025. Accepted: February 25, 2025

© The Author(s) 2025. Published by Oxford University Press on behalf of Nucleic Acids Research.

This is an Open Access article distributed under the terms of the Creative Commons Attribution License (<https://creativecommons.org/licenses/by/4.0/>), which permits unrestricted reuse, distribution, and reproduction in any medium, provided the original work is properly cited.

At least one crossover per chromosome pair is necessary for the accurate segregation of chromosomes during meiosis, a phenomenon known as crossover assurance [3–5]. Failure to generate crossovers can lead to the formation of unbalanced spores, ultimately reducing fertility and potentially causing aneuploidy in the offspring [6].

In plants, as in many eukaryotes, multiple crossover pathways exist, with the dominant one being the class I crossover pathway, driven by a group of proteins collectively known as ZMM [5]. ZMM proteins are essential for creating an environment that stabilizes recombination intermediates and facilitates their resolution into crossovers [7]. In *Arabidopsis thaliana*, the ZMM pathway accounts for at least 85% of all crossovers, so the loss of any ZMM component results in a drastic reduction in both crossover events and fertility [8–11]. In budding yeast, most intermediates stabilized by ZMM proteins result in crossovers, but in many species, like *Arabidopsis*, the number of ZMM-bound intermediates is about 20 times higher than the final number of crossovers [12]. This pathway is also characterized by crossover interference, ensuring that crossovers are more widely spaced along the chromosome than would be expected by random distribution [13, 14]. This regulation of crossover placement is achieved through the ZMM proteins ZYP1 and HEI10. In *Arabidopsis*, the *zyp1* loss of function mutation eliminates crossover interference [15, 16]. Furthermore, the expression level of HEI10 directly affects crossover frequency and the strength of interference [17, 18]. The number of HEI10 foci gradually decreases during prophase I through a process called coarsening, which ultimately determines crossover positions along chromosomes [18–20].

The MutL γ heterodimer, composed of the MLH1 and MLH3 proteins, is regarded as the primary endonuclease responsible for crossover formation within the ZMM pathway [21–24]. Unlike MUS81 and other known endonucleases, which produce crossovers and non-crossovers at a 1:1 ratio, MutL γ exhibits a strong preference for resolving recombination intermediates as crossovers [25–27]. Recent studies in yeast have elucidated the mechanism behind this bias [28, 29]. This unique property of MutL γ ensures that recombination intermediates designated for crossover formation by the ZMM pathway are almost exclusively resolved as crossovers, allowing for precise regulation of crossover numbers necessary to maintain crossover assurance. However, MutL γ complex is typically not classified as an integral component of the ZMM pathway because the mutant phenotypes differ considerably from those of other *zmm* mutants [24, 30]. The number and distribution of MLH1 foci during pachytene are correlated with late recombination nodules and the frequency of class I crossovers [23, 31, 32]. Nevertheless, *Arabidopsis mlh3* mutants show an extensive 25-h delay in prophase I and exhibit only a 60% reduction in crossover numbers, compared to the 85% reduction typically observed in *zmm* mutants [10, 12, 23]. *MLH1* is expressed in both somatic and reproductive tissues, while *MLH3* expression is largely confined to flower buds [23, 33]. Furthermore, both *mlh1* and *mlh3* mutants show partial infertility [23, 33].

In addition to MLH1 and MLH3, PMS1 is another MutL homolog that has been identified in *Arabidopsis*. While the MLH1/MLH3 heterodimer plays a key role in crossover formation, the MLH1/PMS1 heterodimer (MutL α) has been proposed to be involved in the correction of different classes of DNA mismatches [34]. In yeast *pms1* mutants, the fre-

quency of crossovers remains unchanged, but post-meiotic segregation issues arise due to errors in repairing heteroduplexes formed during homologous recombination [22]. In *A. thaliana*, the absence of *PMS1* results in increased somatic ectopic recombination and reduced fertility [35]. However, the meiotic phenotype of *Arabidopsis pms1* mutants has not yet been analyzed.

Class II crossovers, which are insensitive to interference, constitute up to 15% of the total crossovers in *Arabidopsis* and are primarily dependent on MUS81 [9, 11]. Additionally, a second non-interfering crossover pathway has been identified in this species, which depends on FANCD2 [36, 37]. Furthermore, there are anti-recombinase pathways that specifically limit MUS81-dependent crossovers. In *Arabidopsis*, the most effective components of these pathways involve DNA helicases FANCM and RECQ4. Mutants deficient in the genes encoding these proteins exhibit an increase in class II crossovers and a loss of crossover interference [38–41].

In this work, we demonstrate that the function of MLH1 and MLH3 in crossover formation and distribution is significantly different from the role of ZMM proteins. Unlike in *zmm* mutants, crossover interference is still preserved in *mlh1 mlh3* double mutants, although it is strongly affected. Although we cannot exclude that MUS81 plays a role in repairing ZMM-protected recombination intermediates in the absence of MutL γ , it is unlikely to be the only resolvase taking over MutL γ 's function. Moreover, chiasma formation in *mutL γ* mutants is much lower than expected, even when accounting for the absence of crossover bias. Therefore, we suggest that some recombination intermediates in the *mlh1 mlh3* background are ultimately repaired by anti-recombination helicases such as FANCM. In contrast, PMS1 does not seem to be directly involved in crossover formation.

Materials and methods

Plant material: *Arabidopsis* seeds were sown on hydrated soil and stratified in the dark for 48 h at 4°C. They were then cultivated in growth chambers under a 16 h day/8 h night photoperiod, 150 μ mol light intensity, 21°C day and night, and 70% humidity. Col-0 (N1092), Ler-0 (NW20), *hei10-2* (SALK_014624), *mlh1-2* (GK-067E10), *mlh3-1* (SALK_015849), *mlh3-2* (SALK_067953), *pms1-3* (SALK_124014), *fanm-9* (SALK_120621), *zip4-2* (SALK_068052), *mus81-1* (GK-113F11), and *mus81-2* (SALK_107515) were purchased from Nottingham *Arabidopsis* Stock Centre. *mlh1-3* (SK25975) was shared by Raphaël Mercier. *mlh1-1* and *pms1-1* (T-DNA original mutants) were shared by François Belzile. The fluorescent tagged line (FTL) Col-420 was shared by Avraham Levy [42]. The different mutants were genotyped using the primers listed in Supplementary Table S1.

Fertility assays: The seed set was quantified using five siliques starting from the seventh oldest silique of the main stem. The collected siliques were discolored in 96% ethanol and pictured using the Zeiss Lumar V12 Fluorescence Stereomicroscope at the magnification 6.4 \times , then processed using ImageJ. Pollen viability was investigated as previously described [43, 44]. About 500 pollen grains from three replicates (~1500 events total) were processed for each genotype. The mounted samples were observed using the Leica DM4 B at magnification 20 \times .

Seed scoring: Local meiotic crossover recombination frequency (RF) is quantified using the seed-based FTL [45] and the CellProfiler *SeedScoring* pipeline [46]. The frequency of segregation of the two fluorescent cassettes, eGFP and dsRed present at known positions, corresponds to the recombination frequency of the tested line. The *SeedScoring* pipeline recognizes single seed objects and attributes an intensity of fluorescence. The identified objects are categorized as non-color or colored seeds. RF in centimorgan (cM) is calculated as follows: $RF = 100 \times (1 - [1 - 2(N_G + N_R) / N_T]^{1/2})$, where N_G is green-only fluorescent seeds, N_R is red-only fluorescent seeds, and N_T is the total number of seeds.

Cytology techniques: Chromosome spreading was performed from at least three replicates per genotype as described in [47]. The number of univalents, bivalents, and chiasmata were quantified from DAPI-stained pollen mother cells at metaphase I using a Leica DM4 B epifluorescence microscope equipped with a Leica DMC5400 20-megapixel color CMOS camera, previously described [48]. Fluorescence *in situ* hybridization (FISH) was performed as described by Sanchez-Moran *et al.* [49], with minor modifications, on specimens where flower bud fixation and male meiocyte spreading were carried out according to [50]. The DNA probes used were 45S rDNA, pTa71 [12] and 5S rDNA, pCT4.2 [51]. Metaphase I images were scored to determine chiasma frequency and bivalent configurations (ring/rod) per chromosome. The cells were imaged using an Olympus BX61 epifluorescence microscope equipped with an Olympus DP70 digital camera.

CRISPR-Cas9 mutagenesis was used to generate null *mlh1* mutants in Col and *Ler*, as described in [52]. Three sgRNAs were targeted to the region from the fourth intron to the sixth exon of *MLH1*, targeting both splicing variants (Supplementary Fig. S2 and Supplementary Table S2). Four independent mutants were selected and sequenced. Col background mutants showed the same 462 bp genomic deletion, and RT-seq showed a 298 bp deletion at the transcript level, introducing multiple stop codons and a frameshift. *Ler* background mutants showed a single nucleotide insertion in the fifth exon, introducing a frameshift and multiple stop codons.

Lines overexpressing MutL genes were generated by independently introducing extra copies of *MLH1*, *MLH3*, or *PMS1*. Genomic sequences of the different genes were cloned with their respective endogenous promoters or in frame with the meiosis-specific *DMC1* promoter. Cloning primers are listed in Supplementary Table S3. Wild-type plants were transformed using *A. tumefaciens* floral dipping, and transformants were selected using BASTA.

Genome-wide crossover mapping by F₂ sequencing: Whole genome sequencing libraries were constructed based on the protocol described in [48, 53–55]. gDNA was CTAB-extracted from Col/*Ler* F₂ plants rosette leaves (Col × *Ler mlh1* and Col × *Ler hei10-2/+* populations), then isolated using chloroform, precipitated with isopropanol, and purified *via* ethanol precipitation. The obtained gDNA was suspended in TE and its quality and concentration were checked. The samples were diluted to 5 ng/μl and tagged with an in-house produced Tn5 transposase loaded with the Tn5ME-A (5'-TCGTCGGCAGCGTCAGATGTGTATAAGAGACAG-3') or Tn5ME-B (5'-GTCTCGTGGGCTCGGAGATGTGTATAAGAGACAG-3') mixed to Tn5Merev (5'-[phos]CTGTCTCTTATACACATCT-3') linker oligonucleotides, then amplified and indexed using KAPA2G Robust

(Sigma). The PCR products were pooled, size selected (450–700 bp), and purified to obtain a C = [100 ng/μl] and V = 30 μl Novaseq x-plus sequencing sample. The sequencing and demultiplexing was outsourced to Macrogen Europe using pair-end Illumina technology (Supplementary Fig. S4). To identify crossover sites in the examined Col × *Ler mlh1* population and Col × *Ler hei10-2/+*, demultiplexed reads were aligned to the Col-0 genome reference sequence (TAIR10) using BowTie2 [56]. The resultant BAM were sorted with SAMtools v1.2 [57]. The identification of single nucleotide polymorphisms (SNPs) was carried out with SAMtools and BCFtools [58]. SNP calling was based on a comprehensive list generated from a large scale of Col × *Ler* population [59]. The resulting tables of SNPs were filtered to retain only those exhibiting high mapping quality (>100) and high coverage (>2.5×) in R. Libraries with <50,000 reads associated with SNPs were excluded from the analysis. Crossover calling utilized the TIGER pipeline on the filtered files [53]. Finally, crossover distribution frequencies were binned into scaled windows and cumulatively aggregated across chromosome arms. A comprehensive summary of genotyping-by-sequencing (GBS) results is provided in Supplementary Table S4. The raw FASTQ data can be found in the NCBI Sequence Read Archive under the BioProject accession code PRJNA1156934.

Ploidy analysis: Raw reads were aligned to the Col-0 genome reference sequence with BowTie2 [60]. The resulting BAM files were sorted and indexed with SAMtools v1.2 [61]. Mosdepth was used to calculate sequencing depth with the use of -n -fast-mode -b 100 000 parameters [62]. Coverage was plotted for each sample and based on visual inspection; ploidy was determined.

Cis-DCO distances and CoC analysis: Cis-double crossover (*cis*-DCO) distances—defined as the observed distances between parental–heterozygous–parental genotype transitions (i.e. Col/Col–Col/*Ler*–Col/Col and *Ler*/*Ler*–Col/*Ler*–*Ler*/*Ler*)—were computed from GBS data. The frequency of observed distances was compared to the expected frequency of inter-crossover distances under a random crossover distribution. To obtain the expected values, 400 crossover midpoints were randomly selected from all identified crossovers within each genotype, separately for each chromosome. This process was repeated to create a second set of midpoints. For each crossover midpoint in the first set, a midpoint was randomly chosen from the second set, and the distance between them was calculated. Finally, the frequency of events, along with the median of the observed and expected *cis*-DCO distances, was calculated and plotted in 3.5 Mb bins.

To compare the distributions of observed and expected *cis*-DCO distances, gamma distributions were fit to both datasets using the *fitdist* function from the *fitdistrplus* package in R. To assess the statistical significance of the differences between the observed and expected distributions, bootstrap resampling was applied. Specifically, 1000 iterations of bootstrap sampling were performed to estimate the shape parameter (ν) for the gamma distribution of both datasets. In each iteration, a random sample with replacement was drawn from the observed or expected data, and the *fitdist* function was used to fit a gamma distribution to the bootstrap sample. The shape parameter for each bootstrap sample was recorded. The statistical significance of the differences in the shape parameter (ν) between the observed and expected distributions was evaluated using the Mann–Whitney U test, which was applied

to the bootstrap estimates of the shape parameter from both datasets.

For the CoC analysis, expected *cis*-DCO distances were normalized to the observed crossover counts for each genotype as previously described [63]. Then, the observed *cis*-DCO distances were divided by the expected values for each interval separately.

Quantitative RT-PCR analysis: RNA was extracted from *Arabidopsis* unopened flower buds (younger than stage 12) using RNeasy Mini kit (Qiagen). Complementary DNA (cDNA) was obtained using HiScript III 1st Strand cDNA Synthesis Kit + gDNA wiper (Vazyme). The expression levels of genes of interest were measured by qPCR using SYBR™ Green PCR Master Mix (Thermo) and the primers listed in Supplementary Table S5. Both *MLH1* and *MLH3* were analyzed in each of the plants and *Kup9* were used as reference.

Results

The loss of the MutL γ complex has a less severe impact on fertility than the loss of ZMM proteins

The MutL γ complex is widely regarded as the primary resolvase responsible for crossover formation in the class I crossover pathway [3, 4, 6, 64]. Therefore, we decided to check to what extent the lack of genes encoding its components, *MLH1* and *MLH3*, affects plant fertility and crossover formation compared to *zmm* mutants. Since the available mutant alleles of *MLH1* contained either an insertion close to the 3' end of the gene (*mlh1-1*), or in an intron (*mlh1-2*) or upstream of the alternative transcription start site (*mlh1-3*), there was a risk that these were not *null* mutants. Therefore, we used the CRISPR-Cas9 approach to generate an *mlh1-4* mutant *de novo* (Supplementary Figs S1 and S2). We measured the seed set, silique length, and pollen viability in single *mutL γ* mutants, *mlh1-1*, *mlh1-4*, *mlh3-1*, and *mlh3-2*, and compared them to two well-characterized mutants of ZMM genes, *hei10* and *zip4*. While most of the mutants used for this experiment were generated in the Col-0 background, the *mlh1-1* allele originated from the Ws-2 background, therefore both accessions were used as wild-type controls. However, Col-0 and Ws-2 did not differ significantly in fertility, so we considered that *mlh1-1* could be compared with the remaining mutants in the Col background.

Visual inspection of siliques suggests that each of the *mlh1* and *mlh3* mutants is more fertile than *hei10* and *zip4*, although clearly different from wild-type plants (Fig. 1A). Statistical analysis confirmed this observation (Fig. 1B–D): For *mlh1* and *mlh3* mutants, from 17.4 (*mlh1-4*) to 20.7 (*mlh3-1*) seeds per silique were observed on average, and the differences between individual alleles were not statistically significant. In contrast, *zip4* and *hei10* showed only 2.3 and 5.1 seeds per silique, respectively (Fig. 1B). Very similar results were also obtained for silique length (Fig. 1C) and pollen viability (Fig. 1D), although in these assays the *mlh1-4* allele showed a more severe fertility reduction compared to other *mlh* mutants. Interestingly, while the pollen viability in the *mlh* and *zmm* mutants was 59%–73% and 24%–33% of the wild type, respectively, the seed set was only 29%–35% (*mlh*) and 4%–8% (*zmm*) of the wild type (Fig. 1D). This result suggests that egg viability is more significantly reduced than pollen viability. In summary, fertility comparisons show that *mutL γ* mutants

have significantly higher fertility than mutants of genes encoding ZMM proteins.

Given that the dramatic decline in fertility among *zmm* mutants is attributed to a deficiency in crossover, leading to random chromosome segregation during meiosis, we sought to investigate whether crossover frequency is higher in *mlh1-4*. To this end, we examined the number of bivalents in metaphase I (Fig. 1E and F, Supplementary Fig. S3 and Supplementary Table S6). On average, 3.19 bivalents ($n = 57$) were observed in the *mlh1-4* mutant, a statistically significant increase compared to 1.09 in *zip4* ($n = 50$; $P = 2.2E-16$, Welch's *t*-test) and 1.70 in *hei10* ($n = 53$; $P = 3.76E-12$, Welch's *t*-test). The frequency of chiasmata in plants lacking MLH1 was 3.75 (40.5% of wild type), closely comparable to 3.92 reported in *mlh3-1* mutants, which are deficient in MLH1's partner, MLH3 [23]. Based on these results, we concluded that *mlh1-4* mutants, like the previously described *mlh3-1* mutants, generate more crossovers compared to *zmm* mutants, suggesting that some class I crossovers are still produced in the absence of MutL γ .

Local crossover frequencies are significantly reduced in *mutL γ* mutants compared to wild type

To further compare the extent of recombination reduction in *mlh* mutants, we used tester lines where the segregation of linked fluorescent reporters in seeds allows precise measurement of recombination within chromosomal intervals defined by these reporters (Fig. 2A) [42, 45]. For this purpose, *mlh1*, *mlh3*, *zip4*, and *hei10* mutants were crossed with the Col-420 and Col-3.9 lines, enabling the measurement of crossover frequencies in the subtelomeric and pericentromeric regions of chromosome 3, respectively (Fig. 2B). Additionally, the *pms1* mutant was included in the analysis, as PMS1 forms the MutL α heterodimer with MLH1, and we sought to assess its role in meiotic recombination.

Measuring meiotic recombination using the fluorescent seed system was not feasible for *zip4* and *hei10* mutants due to their extremely low fertility and segregation bias. In contrast, the crossover frequency was significantly reduced in *mlh1* and *mlh3* mutants compared to the wild-type control (Fig. 2C). In the 420 interval, all tested *mlh1* and *mlh3* alleles exhibited 14.3–15.9 cM, which was significantly <21.8 cM for the wild type ($P < 1.6E-03$, Welch's *t*-test). In the 3.9 interval, *mlh1* mutants showed 12.2 cM, while *mlh3* mutants showed 14.7 cM, both significantly lower than the wild type's 18.7 cM (Fig. 2C; $P < 2.1E-05$, Welch's *t*-test). Notably, *pms1* showed no changes in crossover frequency at either interval, supporting the hypothesis that the MutL α complex does not influence meiotic recombination (Fig. 2C).

To confirm that the effects of *mutL γ* mutants on crossover formation are not specific to chromosome 3 alone, we also measured recombination in *mlh1-4* and *mlh3-1* mutants at intervals 1.18 and 5.1 located on chromosomes 1 and 5, respectively (Fig. 2B). In both cases, a significant decrease in the crossover rate compared to the wild type was observed, consistent with the observations on chromosome 3 (Fig. 2D). In summary, *mlh1* and *mlh3* mutants exhibit a significantly reduced frequency of meiotic recombination regardless of chromosomal position, while the *pms1* mutation has no effect on crossover formation.

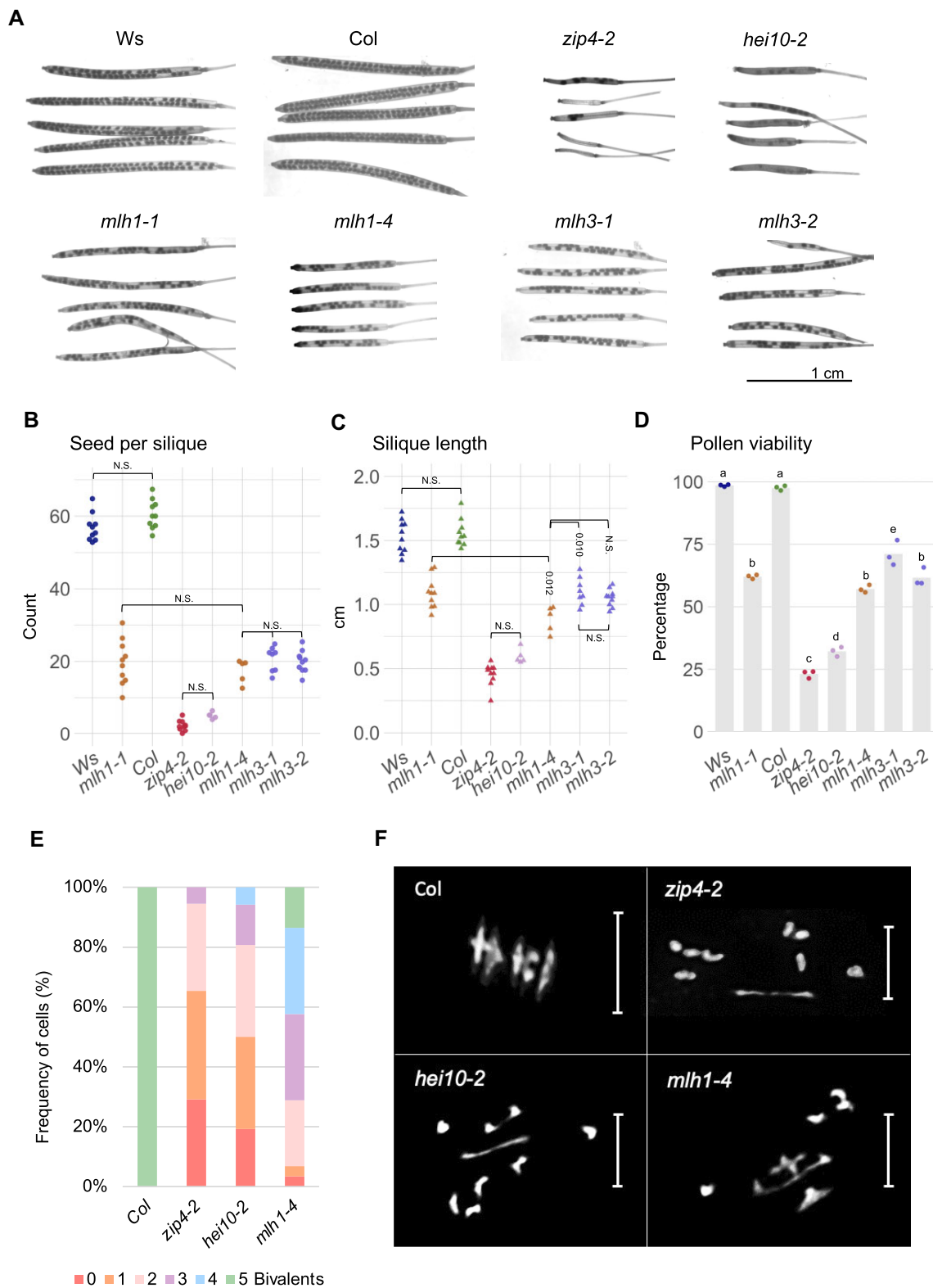


Figure 1. *mutL* mutants exhibit milder fertility and meiotic phenotypes than *zmm* mutants. **(A)** Representative pictures of siliques for wild-type accessions (Ws and Col), *zmm* mutants (*zip4-2* and *hei10-2*), and *mutL* mutants (*mlh1-1*, *mlh1-4*, *mlh3-1*, and *mlh3-2*). Scale bar, 1 cm. Fertility assays for *mutL* mutants compared to the wild types and *zmm* mutants as assessed by seed set **(B)**, silique length **(C)**, and pollen viability **(D)**. The *P* values were estimated using one way analysis of variance (ANOVA) and Tukey HSD tests (Supplementary Tables S10–S12). *n* = 5–10 for panels (B) and (C), and *n* = 3 for panel (D). Cytological characterization of metaphase I meiotic cells showing the frequency of cells with 0–5 bivalents **(E)**, along with representative chromosome spreads from metaphase I meiotic cells for Col (*n* = 27), *zip4-2* (*n* = 53), *hei10-2* (*n* = 50), and *mlh1-4* (*n* = 57) **(F)**. Scale bar, 10 μ m.

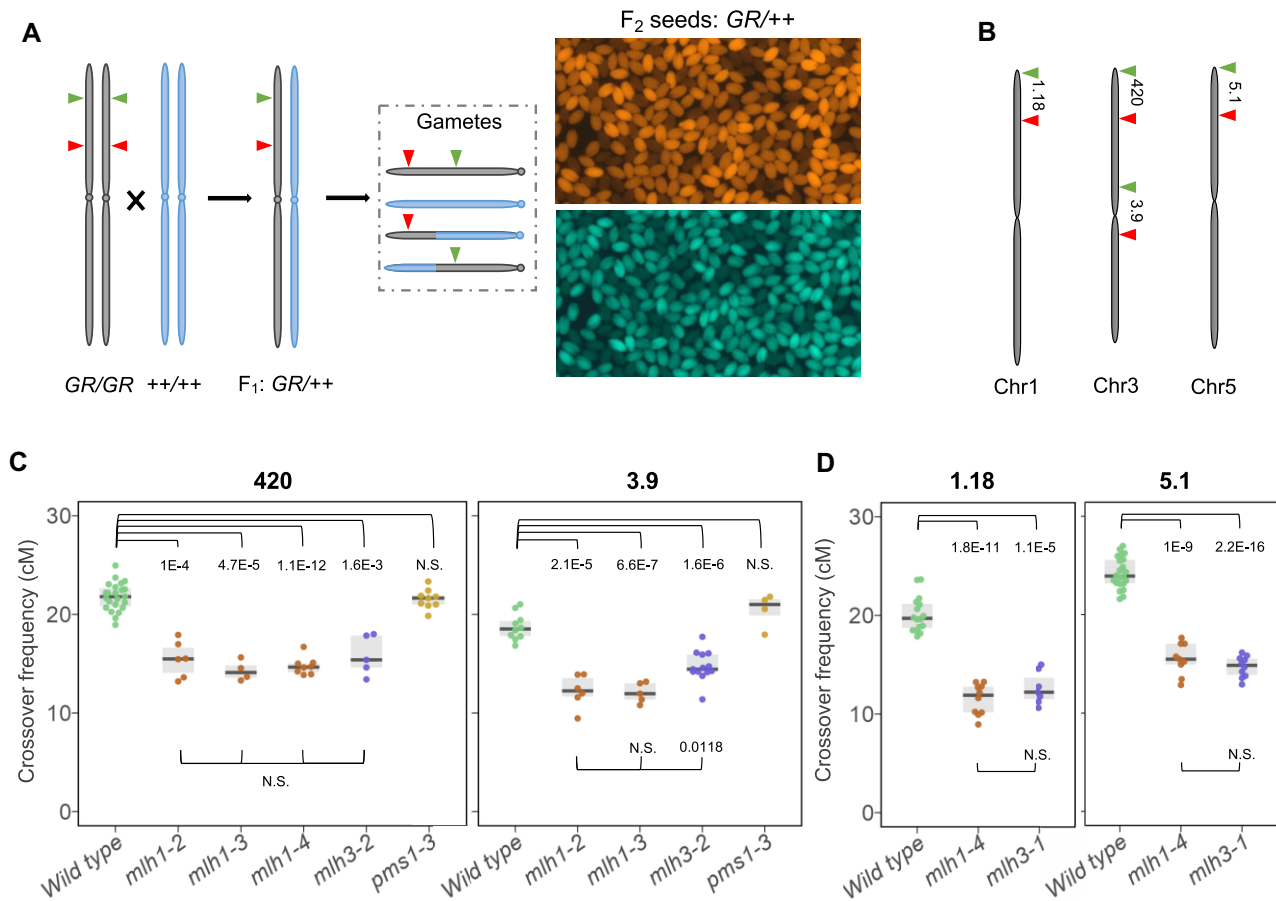


Figure 2. Local meiotic crossover recombination is decreased in *mutL γ* mutants. **(A)** Schematic representation of crossover frequency scoring via fluorescent seed-based system. Arrowheads mark the fluorescent markers delimitating a specific genomic interval. These markers are introduced into the relevant lines via crossing, and recombination frequency is determined by the segregation of the fluorescent markers. **(B)** Chromosome map displaying the fluorescent intervals used in panels (C) and (D). Crossover frequency (cM) for three *mlh1* alleles, two *mlh3* alleles, and one *pms1* allele in the chromosome 3 subteleric region 420 and pericentromeric region 3.9 **(C)**, and for *mlh1-4* and *mlh3-1* in the subteleric regions of chromosome 1 (1.18), and chromosome 5 (5.1) **(D)**. Each dot represents measurements from one individual. The center line of a boxplot marks the median; the upper and lower bounds indicate the 75th and 25th percentiles, respectively. The *P* values were estimated using a Welch's *t*-test.

The progeny of Col/*Ler mlh1* mutants exhibit a notable incidence of trisomy

We aimed to assess the impact of MutL γ loss on crossover distribution across chromosomes and compare it with the distribution observed in *zmm* mutants. To achieve this, we sought to create a comprehensive genome-wide crossover map for the *mlh1* background. Since crossover sites are identified based on genotype switches, generating such a map necessitated sequencing F_2 populations resulting from crosses between two distinct *Arabidopsis* accessions that are polymorphic with respect to each other. Given the absence of an *mlh1* allele in the *Ler* background, we employed the CRISPR-Cas9 method to generate the *mlh1-5* mutant (see [Supplementary Fig. S2](#)). Subsequently, we crossed *mlh1-4* (Col) with the *mlh1-5* (*Ler*) allele and assessed fertility in the resulting F_1 progeny. Of all the ZMM genes, *HEI10* has been shown to be dosage-dependent, and its mutant is haploinsufficient [17]. Therefore, we decided to also use the F_1 cross between *hei10* (Col) and wild-type *Ler* as a control. As expected, seed set and silique length were significantly lower in the *mlh1* Col/*Ler* F_1 compared to the wild type, akin to observations in the *mlh1* Col/Col inbreds, constituting ~28.9% and 63.6% of wild-type values, respectively (Fig. 3A and B). Although mildly affected, the seed set was also

significantly lower in *hei10/+* Col/*Ler*, 88.6% of the wild type ($P = .047$, Welch's *t*-test).

Following self-pollination of the *mlh1* Col/*Ler* F_1 plants, we sequenced the genomic DNA of 288 descendants from a few randomly selected F_1 individuals ([Supplementary Fig. S4](#)). Similarly, we sequenced 225 F_2 from the *hei10/+* Col/*Ler* cross. Because we expected that crossover deficiency in meiosis of F_1 plants would result in random segregation of chromosomes into gametes, we determined the level of aneuploidy in progeny. For this purpose, we examined the sequencing coverage for individual chromosomes in the F_2 individuals and, after normalizing to the total number of reads, we calculated their ploidy level [65]. We adopted a stringent criterion: a ploidy change above $1.2\times$ indicates trisomy, while a change below $0.8\times$ indicates monosomy for a given chromosome. We did not detect any cases of aneuploidy in *hei10/+*. In striking contrast, among 288 *mlh1* Col/*Ler* F_2 individuals, 56 plants exhibited trisomy of chromosome 4, seven plants showed trisomy of chromosome 2, three plants had trisomy of chromosome 5 (Fig. 3C and D, and [Supplementary Fig. S5](#)). Additionally, we observed two cases of simultaneous trisomy of chromosomes 4 and 5, one case of trisomy of chromosome 4 combined with trisomy of the left arm of chromosome 5, and four cases of

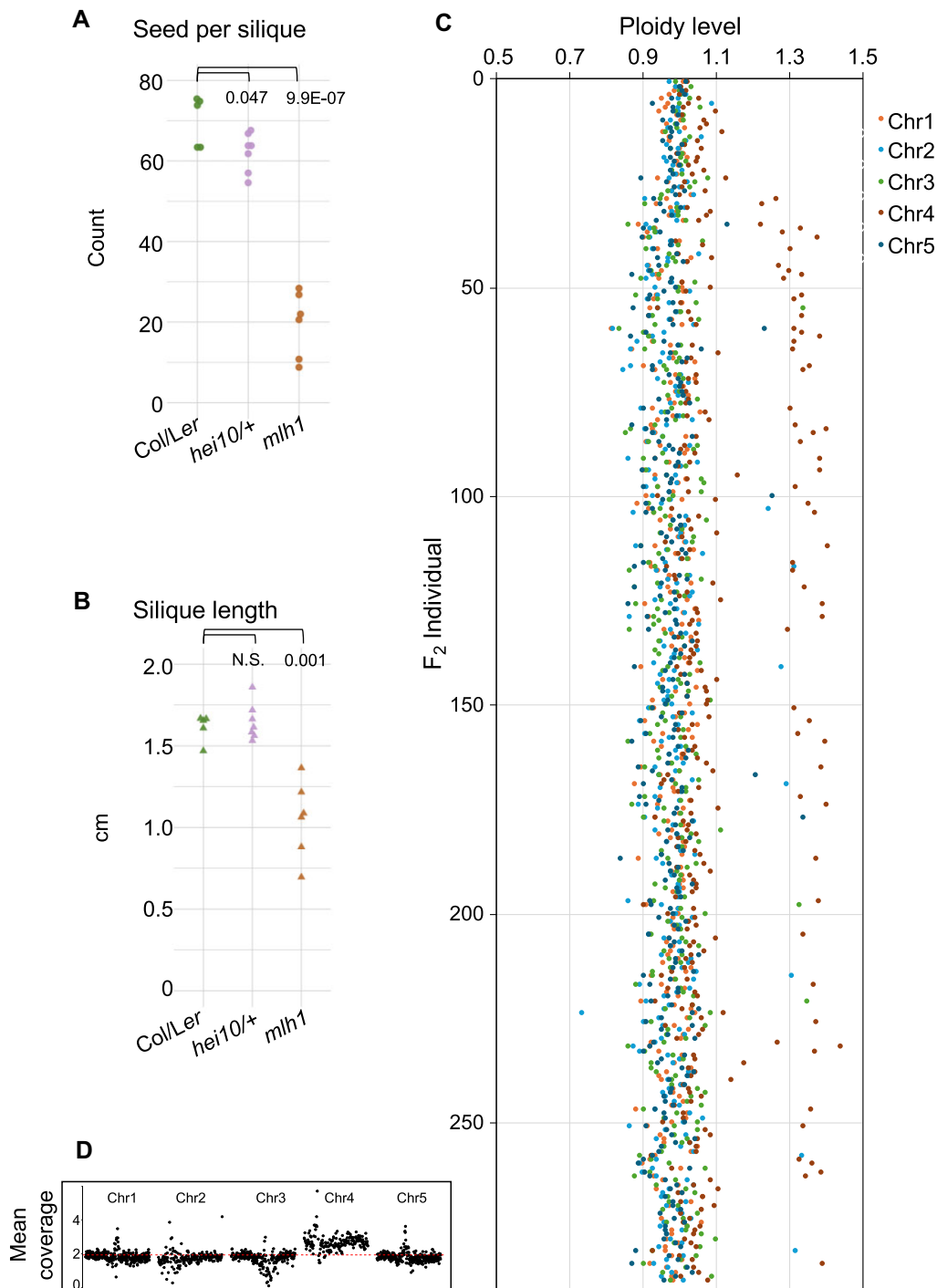


Figure 3. The progeny of *Col/Ler mlh1* mutants exhibit a significant incidence of trisomy. Fertility assays for *hei10-2/+* and *mlh1* mutants compared to the wild-type *Col/Ler* hybrids as assessed by seed set (**A**) and silique length (**B**). The *P* values were estimated using a Welch's *t*-test with $n = 6-7$. (**C**) Ploidy analysis for the *mlh1 Col/Ler* F₂ population as assessed by the ploidy level for each sequenced chromosome in F₂ individuals. (**D**) Example plot illustrating trisomy of chromosome 4, detected based on mean sequencing coverage calculated in 100 kb windows.

partial trisomy of chromosome 4 or 5 (trisomy of an entire arm). Interestingly, no instances of trisomy were observed for chromosome 1.

Only one case of monosomy was found, involving chromosome 2. This low occurrence of monosomics suggests they have more severe detrimental effects, likely due to a greater disruption in gene dosage compared to trisomics (2:1 versus 2:3) [66]. In plants, where the life cycle alternates between

haploid (gametophyte) and diploid (sporophyte) generations, another critical factor may be the complete loss of a chromosome in the meiotic product caused by nondisjunction. Such loss can lead to abnormal gametophyte development [67]. Therefore, we propose that monosomics are subject to stronger negative selection pressures than trisomics.

The high overrepresentation of chromosome 4 in *mlh1* aneuploids is likely due to it being the shortest chromosome, con-

sistent with a recent report on *zyp1* and *zyp1 HEI10* lines, where trisomy was observed exclusively for chromosome 4 [19]. Another reason for the high frequency of aneuploidy of this chromosome in the *mlh1* Col/Ler cross may be the presence of a large 1.2-Mb centromere-proximal inversion differentiating the two accessions [68, 69]. Such a large structural rearrangement could hinder crossover formation for chromosome 4. Given the frequent occurrence of chromosome 4 trisomy compared to other types of aneuploidy in the sequenced F₂ individuals, it is also possible that one of the F₁ plants used was already trisomic. However, the occurrence of various types of aneuploidy is expected as a consequence of the low crossover frequency in *mlh1* mutants. An analogous analysis for the *hei10/+* mutant, which also shows a reduced crossover rate (see below), did not reveal a single case of aneuploidy. We therefore conclude that the reduced recombination frequency in the Col/Ler *mlh1* hybrid results in a higher incidence of aneuploidy.

Comparison of crossover distribution in *mlh1* and *hei10/+* mutants

Genotype distribution analysis along individual F₂ chromosomes allowed us to identify the number and locations of crossovers. To avoid potential biases in crossover distribution caused by aneuploidy, we only included individuals with no evidence of ploidy changes (Fig. 3C). Since only balanced gametes—primarily those that underwent crossovers on all chromosomes during meiosis—can form functional zygotes, the average crossover count estimated from F₂ sequencing may be inflated. Despite this, the total number of crossovers across all chromosomes was significantly lower than in the wild type (Kruskal–Wallis Test $P = 0$; Fig. 4A). Compared to the wild type, *mlh1* mutants showed a more uniform crossover distribution along the chromosomes, with a marked reduction in recombination particularly noticeable in the pericentromeric regions, which are known for relatively high recombination activity in *A. thaliana* (Fig. 4B–D).

The ability to construct a crossover map for plants lacking ZMM is constrained due to the near sterility observed in *zmm* mutants (see *zip4* or *hei10* in Fig. 1A and B). To gain insight into crossover distribution in ZMM-deficient plants, once again we leveraged the dosage-dependency of the *HEI10* gene. We selfed the *hei10/+* Col/Ler plants, sequenced genomic DNA from 225 F₂ individuals, and utilized these data to construct a genome-wide crossover map. The crossover frequency was significantly reduced in *hei10/+* compared to wild-type plants (Kruskal–Wallis Test $P = 1.27E-08$), although it was higher than in *mlh1* ($P = 2.09E-06$) (Fig. 4A). However, the distribution of crossovers in *hei10/+* more closely resembled that in wild type (Spearman $Rho = 0.817$) than in *mlh1* (Spearman $Rho = 0.547$).

Additionally, we compared the chromosomal distribution of crossovers in *mlh1* (and *hei10/+*) with data from other genotypes (Fig. 4E and Supplementary Fig. S6) [17, 55, 59, 70, 71]. Correlations were significantly higher for all genotypes in which class I crossovers predominated ($Rho > 0.472$) than for genotypes with a predominance of class II crossovers ($Rho \leq 0.290$). This result confirms that, despite the absence of MutLγ, the crossovers formed in the *mlh1* mutant exhibit characteristics of class I.

Interference is maintained but weakened in *mlh1*, increased in *hei10/+*, and negative in *msh2 fancm zip4*

The formation of each F₂ individual results from the union of a male and a female gamete, so the analysis of F₂ provides averaged results for both male and female meioses. However, by filtering for the parental–heterozygous–parental genotype (e.g. Col/Col–Col/Ler–Col/Col and Ler/Ler–Col/Ler–Ler/Ler), it is possible to identify *cis*-DCOs and measure DCO distances, which inform about crossover interference [48, 72, 73]. When we compared *cis*-DCOs in *mlh1* to the wild type, we observed that their distances were significantly shorter (Wilcoxon Signed-Rank test $P = 6.7E-03$; Fig. 5A). In contrast, when we compared *cis*-DCOs in *hei10/+*, we found them to be significantly longer than those in the wild type ($P = 2.4E-03$; Fig. 5A).

To examine the role of interference in the genotypes under study, we analyzed the distribution of *cis*-DCO distances and compared it to the expected distribution of distances between two randomly selected crossover sites. In the wild type, *cis*-DCOs with distances up to 7 Mb are underrepresented, while those separated by >10.5 Mb are overrepresented (Fig. 5B). In the *mlh1* mutant, underrepresentation is also observed for *cis*-DCOs with distances up to 7 Mb, but overrepresentation is observed for distances >7 Mb (Fig. 5C). In contrast, the distribution of *cis*-DCO distances in *hei10/+* mirrors the wild type but is shifted further to the right, with the highest overrepresentation of DCOs separated by 14–17.5 Mb (Fig. 5D). These findings demonstrate that although both *mlh1* and *hei10/+* mutants exhibit a reduction in crossover numbers compared to the wild type, they behave differently. In *hei10/+*, the deficiency of the pro-crossover HEI10 protein leads to increased interference, whereas in the *mlh1* mutant, interference is significantly reduced.

We also compared *cis*-DCO distances between the *mlh1* mutant and the *HEI10* overexpressor (*HEI10-OE*), which shows a doubled number of crossovers compared to the wild type and significantly reduced crossover interference [17, 18, 70]. Interestingly, despite the stark difference in crossover numbers between *mlh1* and *HEI10-OE*, there is no significant difference in *cis*-DCO distances ($P = .0858$; Fig. 5A). However, the distribution analysis of *cis*-DCO distances reveals that in the *HEI10* overexpression line, distances above 3.5 Mb are strongly overrepresented, which is not observed in *mlh1* (Fig. 5D and E). This suggests that interference is weaker in *HEI10-OE* than in *mlh1*.

Additionally, we compared *cis*-DCO distances between the *mlh1* mutant and the *msh2 fancm zip4* mutant, for which we recently generated a genome-wide crossover map, although crossover interference had not yet been investigated [55]. Both mutants exhibited very similar seed sets (20.08 in *msh2 fancm zip4* Col/Ler versus 19.57 in *mlh1* Col/Ler) and chiasma counts (3.88 in *msh2 fancm zip4* Col/Col versus 3.75 in *mlh1* Col/Col). However, in *msh2 fancm zip4*, class I crossovers are entirely absent due to the loss of the key ZMM protein ZIP4 [10, 55]. The *cis*-DCO distances were significantly shorter in *msh2 fancm zip4* than in *mlh1* (median = 2.98 Mb versus 7.70 Mb, Wilcoxon Signed-Rank test $P = 4.9E-07$; Fig. 5A). Unexpectedly, the frequency distribution of *cis*-DCO distances in *msh2 fancm zip4* revealed a pronounced overrepresentation of the shortest distances below 3.15 Mb, occurring at twice the expected frequency for a random dis-

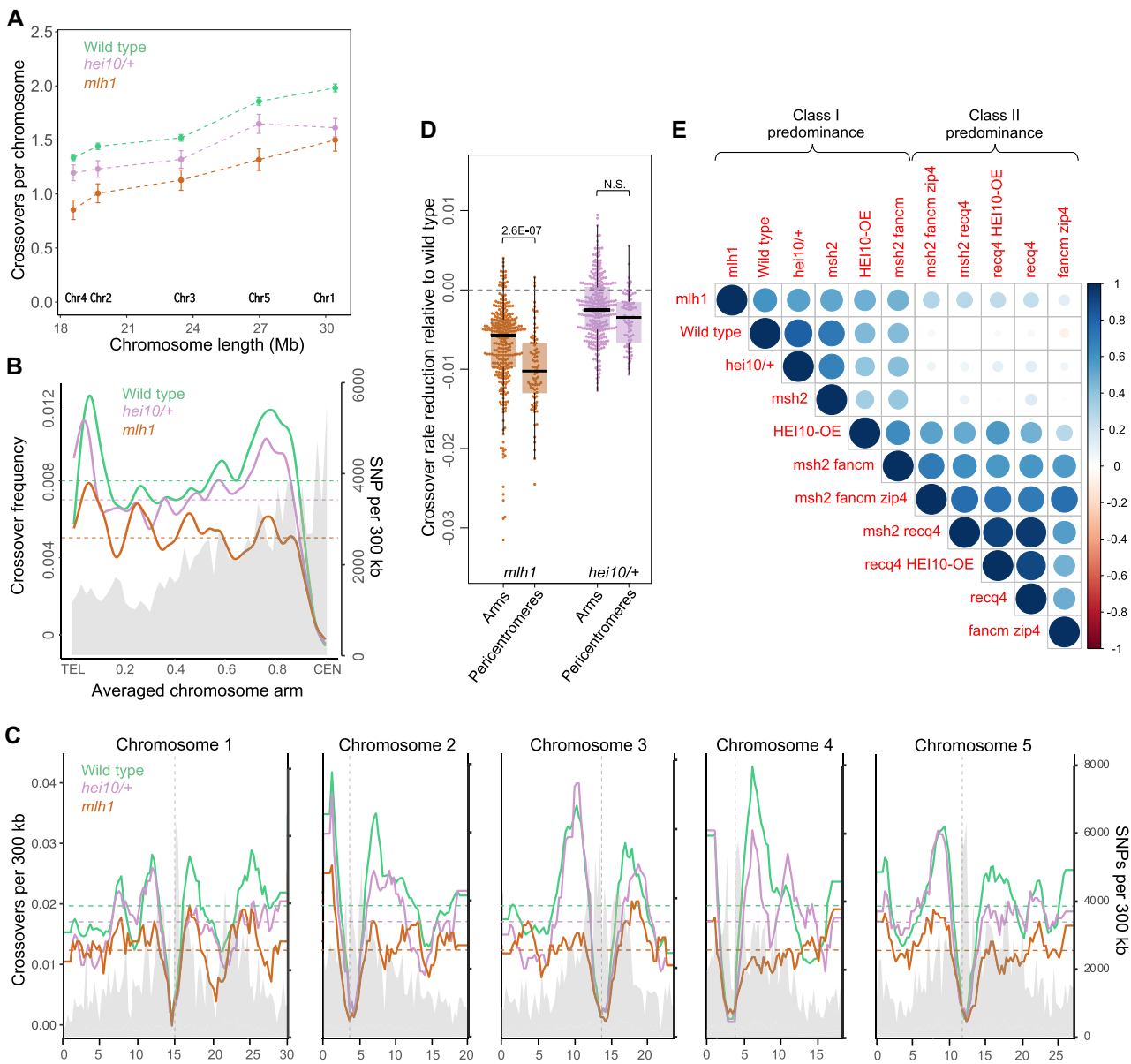


Figure 4. *mlh1* mutants show a reduced number of crossover events genome-wide. **(A)** Differences in total crossover numbers for each chromosome in *mlh1* and *hei10/+* versus wild type. Mean crossover numbers are shown, while whiskers define SEs. **(B)** Comparative representation of crossover frequency per F_2 individual within 300 kb windows, averaged along proportionally scaled chromosome arm, orientated from telomere (TEL) to centromere (CEN). SNP density per 300 kb is shaded in gray. The mean values are shown by horizontal dashed lines. **(C)** Similar to panel (B) but showing crossover frequency plotted along all five *Arabidopsis* chromosomes, averaged in 300 kb windows. Vertical dashed lines indicate centromere positions. **(D)** Relative reduction in crossover frequency within chromosome arms and pericentromeres in *mlh1* and *hei10/+* mutants, versus wild type. Each dot represents a single 300 kb window from panel (C). The center line of a boxplot indicates the median; the upper and lower bounds indicate the 75th and 25th percentiles, respectively. The pericentromeres defined as regions with higher than average DNA methylation, which surround the centromeres. The statistical significance was assessed by one-way ANOVA followed by Tukey HSD test. **(E)** Genome-wide correlation coefficient matrices of crossover distributions, calculated in adjacent 300 kb windows. Data for wild type, *msh2*, HEI10-OE, *msh2 fancm zip4*, *msh2 recq4*, *recq4 HEI10-OE*, *recq4*, and *fancm zip4* from [17, 55, 59, 70, 71].

tribution (Fig. 5F). This indicates that crossover interference in the *msh2 fancm zip4* triple mutant is negative, meaning that crossovers tend to cluster together. The likely cause of this phenomenon lies in the severely altered crossover distribution, which is concentrated almost exclusively at the chromosome ends. Combined with the absence of class I crossovers, this dramatically increases the likelihood of closely spaced events beyond what would be expected in a random distribution.

In summary, our results suggest that MutL γ complexes are not essential for maintaining interference, and the reduced interference observed in *mlh1* is likely due to a proportionally higher number of class II crossovers compared to the wild type. Similarly, interference decreases in the line overexpressing the pro-crossover factor HEI10, but this reduction is attributed to an increased number of crossovers. Conversely, in HEI10 haploinsufficient lines (*hei10/+*), interference increases due to a reduced number of crossovers; however, there are still

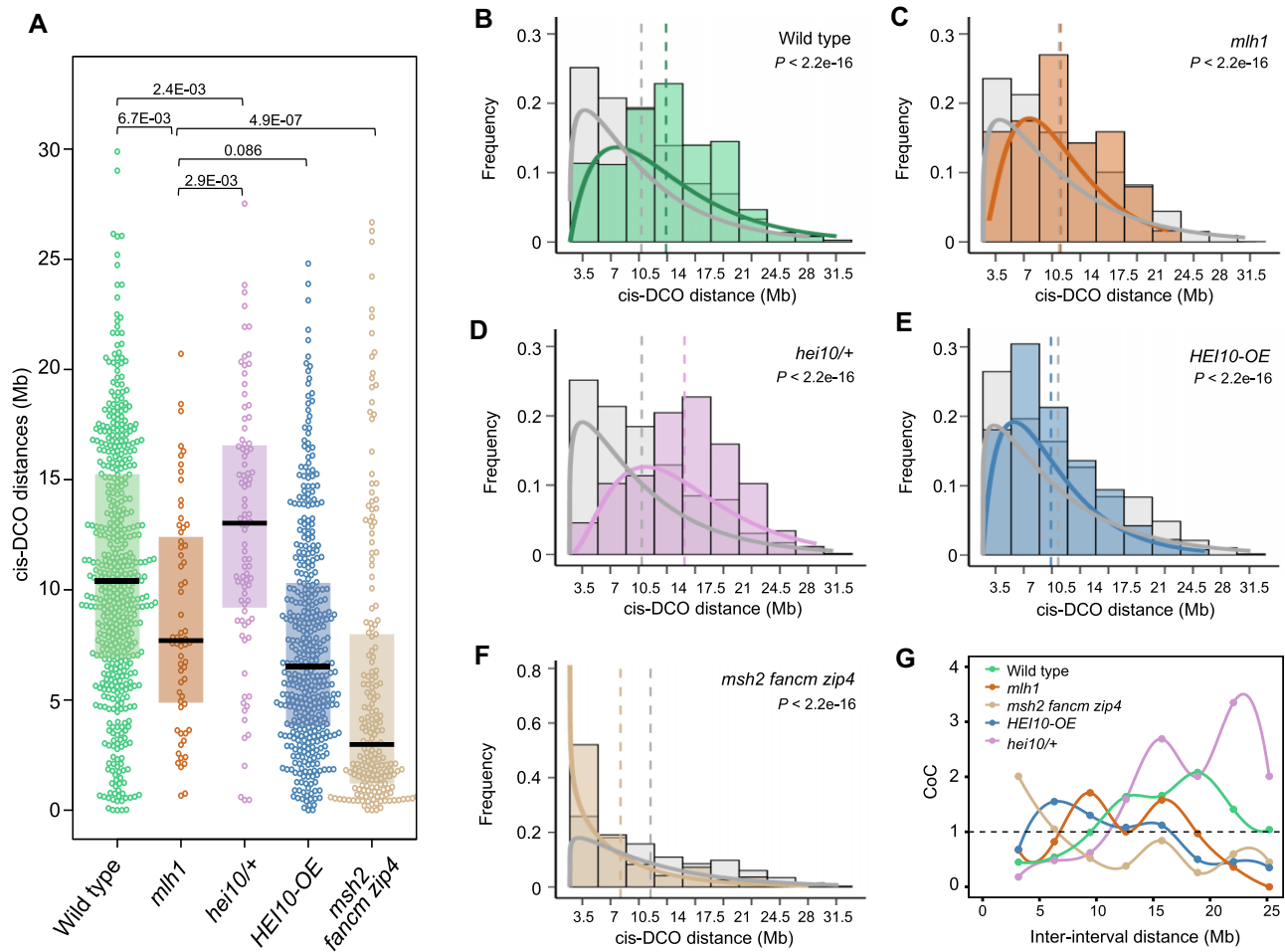


Figure 5. Crossover interference is weakened but maintained in *mlh1*. (A) cis-DCO distances calculated from parental–heterozygous–parental genotype transitions for WT, *mlh1*, *hei10/+*, *HEI10-OE*, and *msh2 fancm zip4*. The center line of a boxplot indicates the median, while the upper and lower bounds indicate the 75th and 25th percentiles, respectively. Each dot represents one cis-inter-crossover distance. The *P* values were estimated using Wilcoxon Signed-Rank test. (B–F) Histograms illustrating the distribution of inter-crossover distances for observed data (colored bars) versus randomly generated distances (gray bars) across five genotypes. The curves represent gamma-fitted distributions for the observed data (colored curves) and the expected data (gray curves). To assess the statistical significance of the differences between the observed and expected distributions, bootstrap resampling was applied to estimate the shape ν parameter, and the Mann–Whitney U test was used to calculate significance. (B) Wild type ($n = 1139$), (C) *mlh1* ($n = 63$), (D) *hei10/+* ($n = 88$), (E) *HEI10-OE* ($n = 404$), and (F) *msh2 fancm zip4* ($n = 194$). Median inter-crossover distances for each genotype are marked with dashed lines in matching colors. Data for panels (B), (E), and (F) from [17, 55, 59]. (G) Coefficient of coincidence (CoC) analysis. The CoC is shown on the Y-axis, with the inter-interval distance in Mb on the X-axis. A CoC value of 1 indicates independent crossover occurrence, while a value near 0 suggests crossover interference.

enough class I events present that class II crossovers do not significantly affect the overall distribution of recombination, thus enhancing interference. In the *msh2 fancm zip4* mutant, only class II crossovers occur, which tend to cluster due to a distribution of events that is highly skewed toward the chromosome ends.

Concomitant loss of MutL γ and MUS81 leads to a significant decrease in fertility and chiasma frequency

Due to the significantly higher chiasma number and fertility of *mutL γ* mutants compared to *zmm* mutants, and the distinct recombination distribution patterns in *mlh1* versus *hei10/+* plants, it appears that another endonuclease partially compensates for the loss of MutL γ . To investigate this, we generated the *mlh1 mlh3 mus81* triple mutant and compared its fertility with other mutants (Fig. 6A and B, and

Supplementary Fig. S7A). Seed set analysis revealed that *mlh1 mlh3 mus81* produces significantly fewer seeds than the *mlh1 mlh3* double mutant (mean = 4.69 and 18.00, respectively; $P = 7.26E-03$, one-way ANOVA and Tukey HSD). Notably, we also observed a slight reduction in seed set in *mus81* compared to the wild-type Col (mean = 51.4 and 60.0, respectively; $P = .021$; Fig. 6A) [11]. Similar trends were observed in the analysis of silique length across *mus81*, *mlh1*, *mlh3* mutants, and their combinations (Supplementary Fig. S7A and Supplementary Table S16). These findings demonstrate that MUS81 plays a critical role when the absence of MutL γ disrupts the proper functioning of the ZMM pathway.

On the other hand, *mlh1 mlh3 mus81* did not produce significantly more seeds than *zip4* (mean = 2.27) and *zip4 mus81* (mean = 0.93) (Fig. 6A). However, drawing conclusions from the comparison of these genotypes is subject to inaccuracy due to very low seed number values. Similarly, silique length shows statistically insignificant differences between these genotypes.

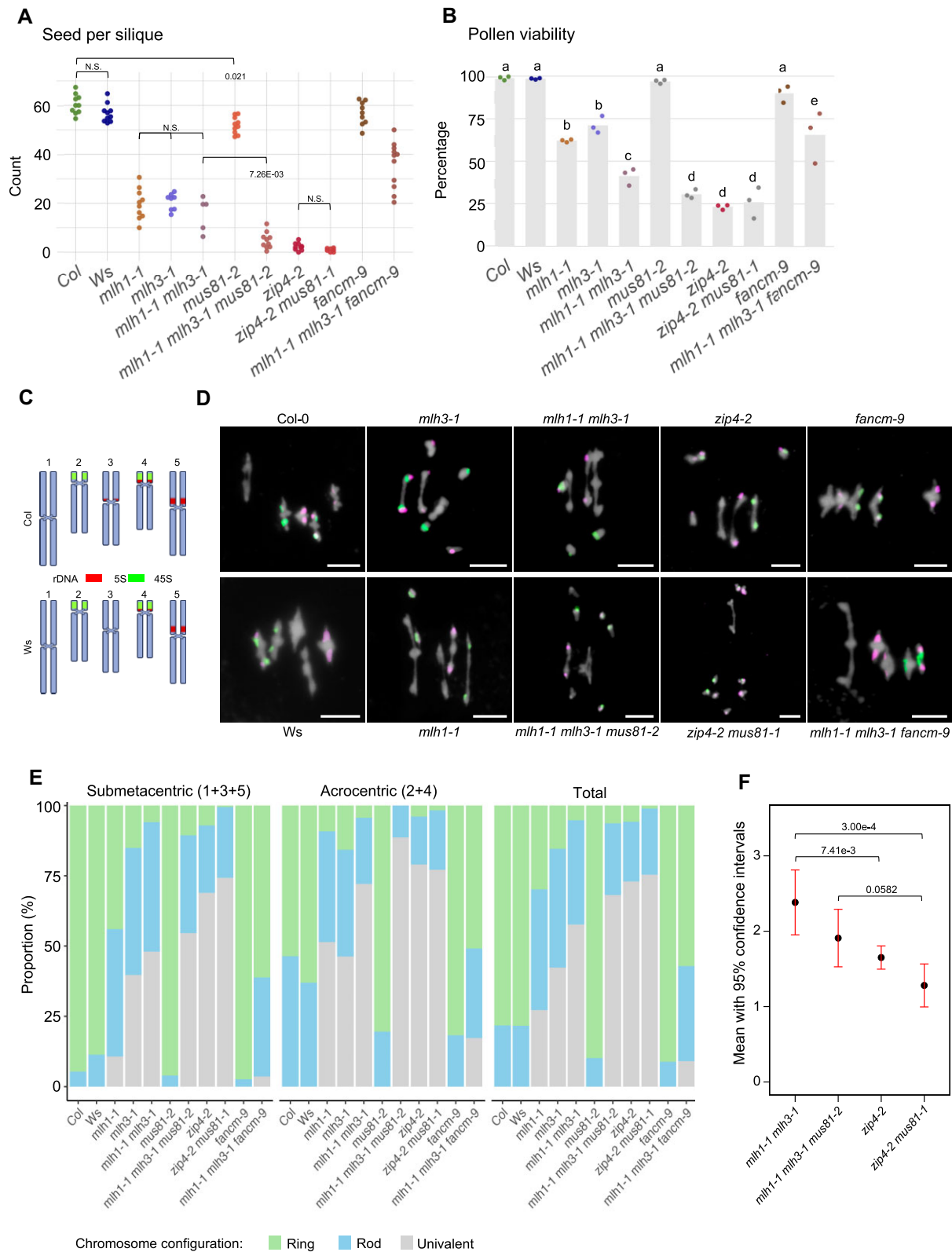


Figure 6. MUS81 endonuclease partially compensates for the loss of MutL γ . Fertility as assessed by seed set (**A**) and pollen viability (**B**). The P values were estimated using one-way ANOVA and the Tukey HSD tests (Supplementary Tables S13 and S14). Sample sizes: $n = 5-11$ in panel (A), and $n = 3$ in panel (B). (C-E) Cytological characterization of metaphase I meiocytes. (C) Chromosome representations of 5S and 45S rDNA positions in Col and Ws genetic backgrounds. (D) Representative pictures of chromosome spreads of metaphase I meiocytes stained with DAPI and labeled with FISH against 5S (red) and 45S (green) rDNA. Scale bar, 10 μm . (E) Frequency of ring, rod, and univalent chromosome configuration in submetacentric chromosomes 1, 3, and 5, acrocentric chromosomes 2 and 4, and the average across all chromosomes. The number of characterized meiocytes for each genotype is as follows: Col ($n = 69$), Ws ($n = 50$), *mlh1-1* ($n = 53$), *mlh3-1* ($n = 108$), *mlh1-1 mlh3-1* ($n = 34$), *mus81-2* ($n = 102$), *mlh1-1 mlh3-1 mus81-2* ($n = 44$), *zip4-2* ($n = 255$), *zip4-2 mus81-1* ($n = 57$), *fancm-9* ($n = 52$), *hei10-2* ($n = 29$), and *mlh1-1 mlh3-1 fancm-9* ($n = 55$). (F) Mean chiasma counts with 95% confidence intervals for selected genotypes. Significance was assessed using a one-way ANOVA with Tukey's HSD test (Supplementary Table S15). Non-significant values are not displayed.

Because seeds are produced by the fusion of two gametes, low seed set and silique length values are the product of reduced viability of both the male and female gametes. Therefore, we also examined pollen viability, the decrease of which in meiotic mutants is a consequence exclusively of impaired male meiosis. We did not observe statistically significant differences between the *mlh1 mlh3 mus81*, *zip4*, and *zip4 mus81* mutants (Fig. 6B). The lack of expected differences between *zip4* and *zip4 mus81* indicates that this analysis is also not precise enough to determine whether MUS81 can contribute to ZMM-mediated crossover repair when MutLγ is absent.

To confirm that the observed decrease in fertility in the *mlh1 mlh3 mus81* mutant compared to *mlh1 mlh3* is due to a further reduction in the number of crossovers, we analyzed bivalent configurations at metaphase I. We used FISH with 5S and 45S rDNA probes to distinguish submetacentric chromosomes 1, 3, and 5 from acrocentric chromosomes and 4 (Fig. 6C and D). This approach enabled us to assess how often individual chromosomes fail to form a chiasma. We evaluated bivalent formation and chiasma count in single, double, and triple mutants (Fig. 6D and E, and Supplementary Fig. S7B and C, and Supplementary Tables S7–S9 and S17). In the *mlh1 mlh3 mus81* triple mutant, we observed a higher total number of univalents than in the *mlh1 mlh3* mutant, which itself had a greater frequency of univalents than the single mutants (Fig. 6E). Notably, the frequency of univalents on acrocentric chromosomes increased by 16.5%, from 72.1% in *mlh1 mlh3* to 88.6% in *mlh1 mlh3 mus81*. In contrast, the increase in univalents on submetacentric chromosomes was only 6.5%, from 48.0% to 54.5% (Fig. 6E and Supplementary Tables S8 and S9). Additionally, no ring bivalents were observed on acrocentric chromosomes in the triple mutant. By comparison, *mus81* and *pms1* mutants showed no significant differences from the control in terms of bivalent configurations and chiasma counting (Fig. 6E and Supplementary Fig. S7C). This increase in univalent numbers in *mlh1 mlh3 mus81* compared to the *mlh1 mlh3* double mutant shows that MUS81 play an important role in resolving joint molecules when MutLγ is not available. Importantly, the *mlh1 mlh3 mus81* mutant displayed fewer univalents and chiasmata than *zip4 mus81* (Fig. 6E and F). This suggests that while MUS81 may potentially act as a resolvase within the ZMM pathway when MutLγ is unavailable, it is not the only endonuclease capable of fulfilling this role.

Knocking out *FANCM* partially improves bivalent formation and rescues the low fertility phenotype in *mutLγ* mutants

The low fertility of *zmm* mutants is caused by a deficiency in crossovers due to the complete disruption of the ZMM crossover pathway. Increasing the frequency of ZMM-independent class II crossovers can restore fertility. In wild-type *Arabidopsis*, class II crossovers are rarely formed because their substrates are typically removed by the activity of DNA helicases like *FANCM* and *RECQ4*. Inactivation of these helicases leads to a significant increase in class II crossovers. Consequently, in *zmm* mutants, the simultaneous loss of *FANCM* or *RECQ4* substantially improves fertility [40, 41, 74].

To test whether the fertility of MutLγ complex mutants could be similarly improved, we generated the *mlh1 mlh3 fancm* triple mutant and compared it with both the *fancm* single mutant and the *mlh1 mlh3* double mutant. The triple

mutant produced an average of 35.8 seeds per silique, significantly more than the 15.7 seeds of the *mlh1 mlh3* mutant ($P = 6.98E-8$, one-way ANOVA and Tukey HSD; Fig. 6A), although still fewer than the wild type (60.5 seeds per silique; $P = 1.43E-11$). A similar increase in fertility has been observed in the *zip4 fancm* mutant [41]. We also examined silique length and pollen viability; these results were consistent with the conclusion that the mutation in *fancm* rescues the fertility of *mutLγ* mutants, as it does for *zmm* mutants (Fig. 6B and Supplementary Fig. S7A).

We then identified individual chromosomes using FISH and examined the bivalent configurations at metaphase I. The *mlh1 mlh3 fancm* triple mutant exhibited over six times fewer univalents and >10 times as many ring bivalents compared to the *mlh1 mlh3* double mutant, indicating a significant increase in crossover frequency (Fig. 6E and Supplementary Fig. S7C and Supplementary Tables S7–S9). Interestingly, univalents were over four times more common on acrocentric chromosomes compared to submetacentric ones in the *mlh1 mlh3 fancm* mutant, accounting for 17.3% and 3.6%, respectively (Fig. 6E and Supplementary Table S8 and Supplementary Table S9). This suggests a lack of crossover assurance, consistent with the observed increase in class II crossovers in this mutant.

Overall, these data show that, similar to *zmm* mutants, the loss of *FANCM* in *mutLγ* mutants also increases crossover frequency, which contributes to their improved fertility. However, despite this increase, the triple mutant had a lower frequency of ring bivalents (57.1%) compared to the control (78.3%), and univalents persisted. This suggests that, unlike in *zmm* mutants, the *fancm* mutation does not fully restore the chromosomal configurations seen in the control in the *mlh1 mlh3* background.

Elevated expression of *MLH1* or *MLH3* causes a moderate increase in crossover frequency

We sought to determine whether increasing the expression of *MLH1*, *MLH3*, and *PMS1* would affect crossover frequency. To this end, we cloned the genomic sequences of these genes under their native promoters and transformed them individually into Col-420 plants hemizygous for fluorescent crossover reporters (Supplementary Fig. S8). T₁ plants segregating for the 420 reporters were used to assess crossover frequency within this interval. Most T₁ plants exhibited crossover frequencies similar to the wild type, with no significant changes observed in the T₂ generation following selfing (Supplementary Fig. S9A and B). For selected *pMLH1::MLH1* and *pMLH3::MLH3* T₂ plants, we isolated RNA from closed flower buds and measured gene expression levels using RT-qPCR. We observed that the expression level in these lines was 1.8–14.4 times higher than in wild-type plants, demonstrating that increasing the expression of a single *MLH* gene does not significantly affect crossover frequency (Supplementary Fig. S9C).

In parallel, three independent T₂ plants for both *MLH1* and *MLH3* constructs were crossed with Col-420 or *Ler* to generate F₁ inbred (Col × Col-420) and F₁ hybrid (Col-420 × *Ler*) progeny (Supplementary Fig. S8). Crossover frequency measurements in the 420 interval revealed that crosses carrying additional copies of *MLH1* exhibited a significant increase in recombination in the inbred background, though this effect was not observed in hybrids with *Ler* (Fig. 7A). In these

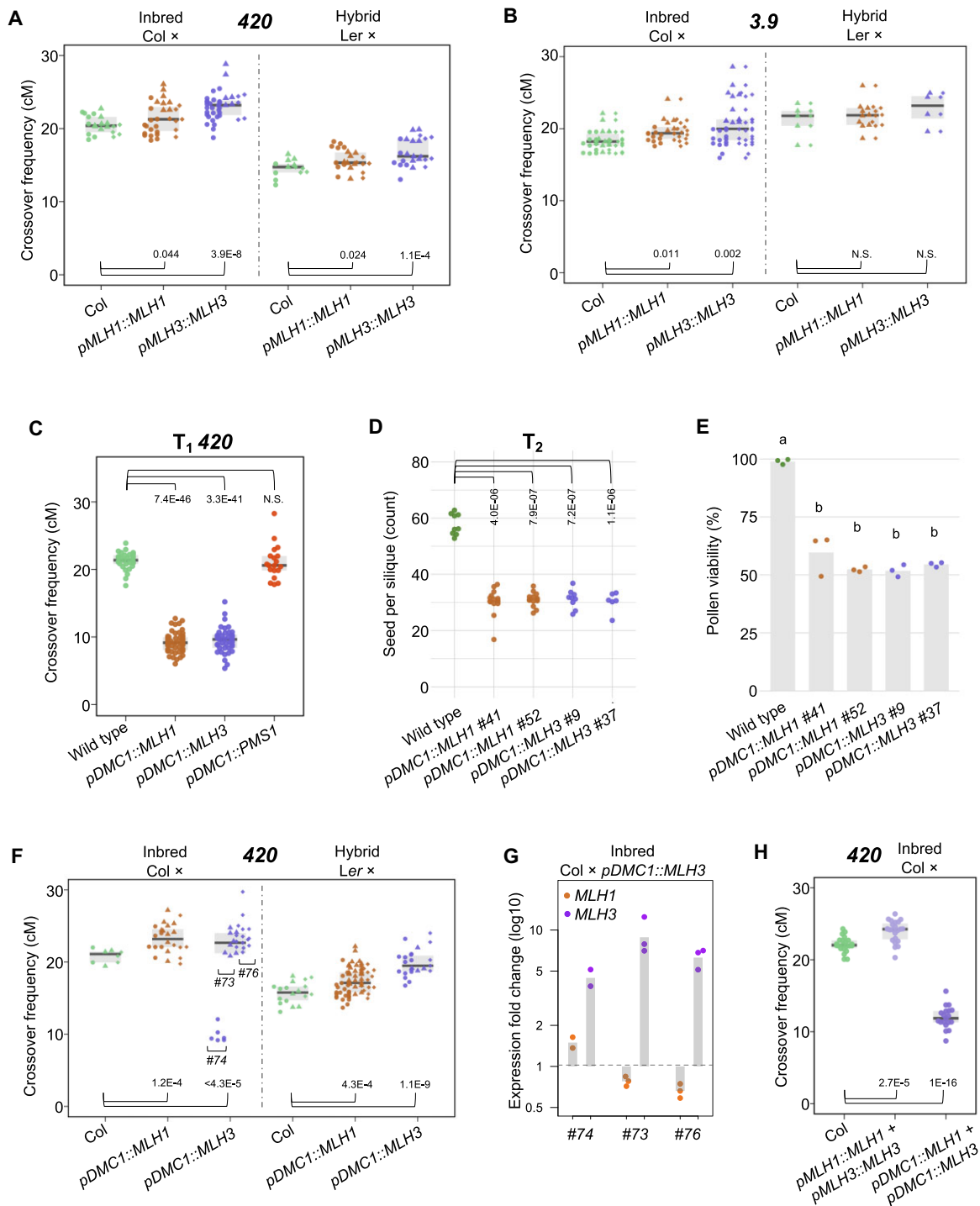


Figure 7. Increased MutL γ expression boosts crossovers, but its misregulation drastically reduces crossover numbers and plant fertility. **(A)** Crossover frequency in inbred Col/Col and hybrid Col/Ler F₁ plants with additional *MLH1* or *MLH3* copies under their respective native promoters, measured in 420 subtelomeric region of chromosome 3. Each data point represents a measurement from one plant. Independent transformant lines for each genotype are indicated by a different data point shape. **(B)** As for panel (A) but measured in 3.9 pericentromeric region. **(C)** Crossover frequency of *MLH1*, *MLH3*, and *PMS1* overexpressors under the control of *DMC1* promoter at the T₁ generation, measured in 420. Each data point represents a measurement from one plant. **(D)** Fertility assays for *MLH1* and *MLH3* overexpressors, under *DMC1* promoter, assessed by seed set. Each data point represents the average of five siliques from a single plant. The *P* values were estimated using one-way ANOVA and the Tukey HSD tests (Supplementary Table S18). **(E)** As in panel (D) but showing pollen viability. Each data point represents a measurement of 500 pollen grains from one plant. The *P* values were estimated using one-way ANOVA and the Tukey HSD tests (Supplementary Table S19). **(F)** Crossover frequency in inbred Col/Col and hybrid Col/Ler F₁ plants overexpressing additional *MLH1* or *MLH3* copies under *DMC1* promoter, measured in the 420 interval. **(G)** Expression levels in F₁ Col \times pDMC1::MLH3 plants shown in panel (F) as determined via RT-qPCR for both *MLH1* and *MLH3* in each plant. Each dot represents one biological replicate (one cross of a T₂ plant). Bar plots show the average fold change relative to wild type. **(H)** Crossover frequency in inbred Col/Col F₁ plants with additional *MLH1* and *MLH3* copies (double overexpressors) under their native or *DMC1* promoter, measured in the 420 interval. In this figure each dot represents a measurement from one individual. For crossover frequency (**A–C**, **F–H**), the center line of a boxplot indicates the median; the upper and lower bounds indicate the 75th and 25th percentiles, respectively, and the *P* values were estimated using the Welch's *t*-test.

crosses, *MLH1* and *MLH3* expression levels were similar to those observed in the T₂ generation (Supplementary Fig. S9D). We also repeated this experiment for the 3.9 interval, which allows measurement of crossover frequency in the pericentromeric interval (the location is shown in Fig. 2B), and obtained very similar results (Fig. 7B). Interestingly, a significant increase in recombination frequency was observed in both inbred and hybrid backgrounds for lines with additional copies of *MLH3* (Fig. 7A), suggesting that elevated *MLH3* expression enhances crossover rates regardless of genetic background.

Incorrect expression of *MLH1* or *MLH3* inhibits crossover recombination and impacts fertility

Since some T₁ plants showing increased expression of *MLH1* or *MLH3* also exhibited reduced fertility (Supplementary Fig. S9D–F and Supplementary Tables S20 and S21), we hypothesized that an excess of these proteins might be toxic for the cell. To verify this hypothesis, we modified the genetic constructs for the *MLH1*, *MLH3*, and *PMS1* genes by substituting their promoters for the promoter of the *DMC1*. The *DMC1* recombinase serves as a meiosis-specific RAD51 homolog [75]. Importantly, *DMC1* functions at significantly earlier stages of meiotic recombination compared to MutLγ, and thus its expression is assumed to occur before *MLH3* [76]. Subsequently, we transformed 420 segregating plants with these modified constructs and assessed crossover frequency. Remarkably, virtually all T₁ plants carrying the *pDMC1::MLH1* and *pDMC1::MLH3* constructs displayed a significantly reduced crossover frequency, plummeting from ~22 cM in the wild type to only ~10 cM in T₁ (Fig. 7C). Conversely, no such effect was observed for plants with the *pDMC1::PMS1* construct, confirming the negligible role of *PMS1* in meiotic recombination (Fig. 7C).

The T₂ generation plants also showed a reduced 420 crossover frequency (Supplementary Fig. S10B). Additionally, fertility assessments conducted on T₂ plants carrying the *pDMC1::MLH1* and *pDMC1::MLH3* constructs revealed a notable decrease in seed set and pollen viability, dropping to ~50% of the level observed in the wild type (Fig. 7D and E). We did not observe any phenotypic changes at the level of vegetative development or in the structure of flowers. We examined the expression levels in independent T₂ lines carrying *pDMC1::MLH1* and *pDMC1::MLH3*. In *pDMC1::MLH1* lines, the *MLH1* expression levels increased 2.9- to 4.2-fold compared to the native expression observed in wild-type plants and were associated with a decrease in *MLH3* expression (Supplementary Fig. S10A). In contrast, a substantially higher increase in *MLH3* expression compared to wild type were observed in *pDMC1::MLH3* lines (11.3- to 63.6-fold), which was associated with an increase in *MLH1* expression (Supplementary Fig. S10A). Compared to lines with endogenous promoters, lines with overexpression driven by the *DMC1* promoter exhibit deregulation of the transcript levels of the second MutLγ component gene (*MLH3* for *pDMC1::MLH1* lines and *MLH1* for *pDMC1::MLH3* lines, respectively).

Three independent T₂ plants, for which we examined the expression levels, were subsequently crossed with Col-420 and *Ler* to assess recombination in both inbreds and hybrids (Supplementary Fig. S8). In the resulting F₁ plants, the 420 crossover frequency was measured, which, in some in-

stances, surpassed that of the wild-type control (Fig. 7F). For F₁ inbreds, we analyzed the expression levels of both genes in these lines. In the case of *pDMC1::MLH1*, *MLH3* expression increased in F₁ compared to T₂ ($P = .04948$, Welch test), approaching wild-type levels. Conversely, for *pDMC1::MLH3*, *MLH1* expression decreased, also nearing the native level ($P = .00338$, Welch test; Supplementary Fig. S10C). We argue that crossing with a wild-type plant brings the expression level of the coregulated MutLγ component (*MLH3* for *pDMC1::MLH1* and *MLH1* for *pDMC1::MLH3*) closer to a point that no longer reduces crossover frequency or compromises fertility. Notably, in one line carrying the *pDMC1::MLH3* construct, #74, recombination decreased to 10 cM in inbred, akin to the level observed in self-pollinated T₂ plants. Interestingly, among the three *pDMC1::MLH3* × Col crosses analyzed for expression levels, only cross with line #74 showed an increased expression of *MLH1* (Fig. 7G). These observations underscore the sensitivity of MutLγ components to expression levels.

Because the MutLγ complex is a heterodimer containing both *MLH1* and *MLH3*, we decided to investigate how meiotic recombination would be affected by simultaneous increase in the expression of both genes. To this end, we crossed T₂ plants carrying additional copies of *MLH1* and *MLH3*. Due to the reduced fertility of T₂, only a small proportion of crosses were successful. Pooled F₁ from three crosses between independent T₂ plants with additional copies of *MLH1* and *MLH3* under their native promoters showed an increased 420 crossover frequency (Fig. 7H; 23.94 cM versus 22.11 cM for wild-type control; $P = 1.27E-05$, Welch's *t*-test). However, in double overexpressor plants with additional genes driven by the *DMC1* promoter, recombination was significantly lower than in the wild type, as was the case in single overexpressors (Fig. 7H; 11.97 cM; $P = 6.72E-22$). These results show that simultaneous upregulation of both genes of the MutLγ complex does not result in significant changes in recombination rates compared to those observed in single overexpressors. In conclusion, modifying the expression of MutL complex genes cannot be routinely used to increase recombination frequency because plants are highly sensitive to the levels of *MLH1* and *MLH3* in the cell. Incorrect expression is often toxic and can lead to a drastic decline in fertility.

Discussion

The MutLγ complex is widely regarded as the main resolvase for class I crossovers, which depend on ZMM proteins (hence the name ZMM crossover pathway) [3, 5, 6]. Despite their role in this pathway, *MLH1* and *MLH3* are not classified as ZMM proteins, and their role in the pathway, aside from functioning as a resolvase, remains unclear. The primary reason for excluding MutLγ from the ZMM group lies in the distinct phenotypic differences: in many eukaryotes, mutants lacking components of the MutLγ complex exhibit a milder phenotype compared to classical ZMM mutants, displaying higher fertility and an increased crossover frequency [30, 77, 78–81]. In this study, we undertook a comprehensive characterization of the MutLγ complex in *A. thaliana*, employing a diverse set of methodologies.

We analyzed plant fertility and bivalent formation during meiosis in various alleles of *mlh1* and *mlh3*, including the *mlh1-4* null allele generated using CRISPR-Cas9 technology (this study). As expected, all mutants showed reduced fertility

and fewer bivalents than the wild type, but the defects were less severe than in the ZMM mutants *zip4* and *hei10* (Fig. 1) [23, 33, 82]. Fluorescent seed-based measurement of crossover frequency in chromosomal intervals showed a decrease in recombination in both pericentromeric and subtelomeric regions in *mlb1* and *mlb3* mutants (Fig. 2). Notably, the *pms1* mutant, a component of the MutL α complex, did not show significant changes compared to the wild type, confirming that it does not play a significant role in meiotic recombination (Fig. 2) [35].

We also generated genome-wide crossover maps for *mlb1* to assess its similarity to ZMM mutants. To further investigate this, we constructed a crossover map for the *hei10/+* mutant, the only ZMM mutant with a dosage effect (as homozygous mutants are nearly infertile, making crossover analysis unreliable) [17, 83]. Since reduced crossover numbers can lead to aneuploidy, we first examined the ploidy levels in F₂ plants through sequencing. While no aneuploids were found in *hei10/+*, a significant number were present in *mlb1* F₂ plants (Fig. 3C and D). The *mlb1* mutant exhibits a different recombination pattern compared to *hei10/+* and wild type, showing a more even distribution of crossovers along chromosomes, particularly noticeable along the chromosomal arms (Fig. 4B and C). In contrast, crossover patterns in *hei10/+* are similar to wild type, with pronounced increases in pericentromeric and subtelomeric regions (Fig. 4B and C). We further compared these patterns with other genotypes analyzed through the same method (Fig. 4E) [17, 55, 59, 70, 71]. These comparisons revealed that the crossover distribution in *mlb1* resembles class I crossover patterns rather than class II. This suggests that many crossovers in *mlb1* exhibit class I characteristics, and the observed deviations from wild-type distribution may stem from a reduced class I/class II ratio.

Interestingly, in the *mlb1* mutant, the reduction in crossover frequency was significantly more pronounced in pericentromeric regions compared to chromosome arms (Fig. 4B and D), a pattern observed only marginally in the *hei10/+* mutant (Fig. 4B and D). The most plausible explanation for this phenomenon is the relatively higher proportion of class II crossovers in the *mlb1* background. Class II crossovers are known to be inhibited by interhomolog polymorphism, which likely causes them to preferentially form farther from polymorphic centromeric-proximal regions [55]. Alternatively, this result might indicate that the ability of the ZMM pathway to form crossovers in polymorphic regions depends on MutL γ , suggesting that its substitution by another resolvase is not effective in these contexts.

Shorter distances between crossover pairs indicate weaker interference [72]. In addition to our data for *mlb1* and *hei10/+*, we analyzed previously published datasets (not yet evaluated for *cis*-DCO distances) for lines overexpressing *HEI10*, as well as the *msh2 fancm zip4* mutant and wild type [17, 55, 59]. The *hei10/+* mutant showed increased interference compared to wild type (Fig. 5A and D), consistent with the known pro-crossover role of HEI10 and the coarsening model of crossover interference. In this model, reduced HEI10 availability limits the number of HEI10 foci that can mature into class I crossovers, thus enhancing interference [18, 20]. Conversely, *HEI10* overexpression led to decreased interference, as more HEI10 foci matured into crossover-competent foci (Fig. 5A and E), aligning with previously published results on crossover interference in this line [18, 70].

The *mlb1* mutant exhibited significantly shorter *cis*-DCO distances compared to wild type, indicating reduced in-

terference (Fig. 5). Notably, *cis*-DCO distances in *mlb1* were not significantly different from those in the *HEI10*-overexpressing line, despite an approximately four-fold difference in crossover numbers between these genotypes. This suggests that the mechanism of interference reduction in *mlb1* is distinct from that in *HEI10* overexpression. In *mlb1*, the reduction appears to stem from the loss of the primary resolvase in the ZMM pathway, while other pathway components remain intact [18, 70]. We propose that the main cause of reduced interference in *mlb1* is the altered class I/class II crossover ratio, driven by the drastic reduction in class I crossovers.

Based on this conclusion, we hypothesized that interference in the *mlb1* mutant is not abolished because some recombination intermediates, protected by ZMM proteins, are resolved into crossovers by alternative nucleases. To test this hypothesis, we compared *cis*-DCO distances in the *mlb1* mutant with those in the *msh2 fancm zip4* mutant. In this latter mutant, class I crossovers cannot form due to the *zip4* mutation, while class II crossovers are elevated by the loss of the anti-crossover helicase FANCM and inactivation of the mismatch sensor MSH2 [10, 41, 55]. Interestingly, despite both mutants exhibit similar fertility and crossover numbers, the *msh2 fancm zip4* mutant showed significantly shorter *cis*-DCO distances than *mlb1* (Fig. 5). This difference arises because class II crossovers in *msh2 fancm zip4* are not subject to interference. These results support the idea that while crossover interference is reduced in the *mlb1* mutant, it remains functional.

We also performed extensive genetic interaction studies involving *mlb1* and *mlb3* in combination with other meiotic recombination mutants. By analyzing fertility and chiasma numbers, we confirmed that another nuclease partially compensates for the loss of MutL γ in mutants lacking MLH1 and/or MLH3 (Fig. 6). A comparison of meiosis progression reveals that prophase I in *mlb3* lasts three times longer than in *msh4* [12, 23]. This extended duration may provide additional time for an alternative nuclease to repair ZMM-protected recombination intermediates through crossover formation. The most obvious candidate for this role is the structure-specific nuclease MUS81. However, while the *mlb1 mlb3 mus81* mutant shows a higher frequency of univalents and fewer chiasmata than the *mlb1 mlb3* mutant, these differences are almost identical to those observed between *zip4 mus81* and *zip4* alone (Fig. 6E and F), likely reflecting the role of MUS81 that is independent of ZMM. Among the mutants compared, *zip4 mus81* exhibits the highest frequency of univalents and the lowest number of chiasmata. Therefore, while we cannot rule out the possibility that MUS81 may partially take on the role of a resolvase in the absence of MutL γ , it is clear that it is not the sole enzyme fulfilling this function.

Unlike MutL γ , other resolvases do not exhibit crossover-biased resolution and generate crossovers and non-crossovers at equal frequencies [24, 27]. However, the *mlb1-4*, *mlb3-1*, and *mlb1-1 mlb3-1* mutants we analyzed show lower-than-expected chiasma frequencies, even when accounting for unbiased resolution. This suggests inefficiency in resolving ZMM-protected intermediates. Therefore, we propose that some recombination intermediates are ultimately repaired through the action of DNA helicases and RTR complexes (RecQ4/Top3 α /RMI, homologous to human BTR).

We found that the mutation of the anti-crossover DNA helicase FANCM significantly mitigates the effects of MutL γ loss (Fig. 6). It is already established that FANCM suppresses

mutations in *zip4* and other ZMM genes [41, 74, 84–86]. However, the findings regarding the mutant lacking MutL γ are particularly noteworthy because the ZMM complexes remain fully functional, with only the main resolvase absent. It is widely accepted that ZMM proteins protect recombination intermediates from the actions of DNA helicases and structure-specific nucleases [6, 27, 87]. Thus, we conclude that in the presence of ZMM proteins and in the absence of MutL γ , class II crossovers can still occur in regions occupied by ZMM.

We also examined how increasing the expression of MutL γ components influences crossover frequency. A moderate increase in *MLH3* expression resulted in a modest rise in crossover frequency in both subtelomeric and pericentromeric regions (Fig. 7). The effect of *MLH1* was less pronounced, indicating that *MLH3* may be the limiting factor within the MutL γ complex. This is consistent with the significantly lower native expression of *MLH3* compared to *MLH1*, as well as the meiosis-specific nature of *MLH3* [23]. Additionally, the meiotic phenotypes of the single mutants differ, with *mlh3* exhibiting a higher frequency of univalents and rod bivalents compared to *mlh1* (Fig. 6). However, *DMC1* promoter-driven overexpression of either *MLH1* or *MLH3*—unlike *PMS1*—resulted in a drastic reduction in both crossover frequency and plant fertility. Interestingly, we observed deregulation of both *MLH1* and *MLH3* gene expression in these lines. However, it is difficult to definitively determine whether this is the cause of the decrease in crossover frequency. Recent studies in yeast have revealed an unexpected interaction between *MLH1*–*MLH3* and the recombinase *DMC1* [88]. It is possible that premature overexpression of MutL γ components leads to competition with *DMC1*, thereby restricting proper strand invasion and/or the formation of early recombination intermediates. This highlights the need for strict regulation of *MLH1* and *MLH3* protein levels during meiosis. In contrast, our findings suggest that *PMS1* does not play a significant role in meiotic recombination.

Acknowledgements

We thank Avi Levy (The Weizmann Institute, Israel) and Scott R. Poethig (University of Pennsylvania, US) for FTLs (CTLs); François Belzile (Université Laval, Canada) for sharing *mlh1-1* and *pms1-1*, Raphaël Mercier (Max Planck Institute for Plant Breeding Research, Germany) for sharing *mlh1-3*; Franz Boideau for help with CoC analysis. B. Martín, M.C. Moreno, J. Barrios, and H. Korcz-Szatowska for their excellent technical assistance.

Author contributions: N.K., J.L.S., M.P., and P.A.Z. designed the research; N.K., N.F.J., W.D., A.P., E.S.Z., A.M.V., and J.D. performed the experiments; W.D. performed the computational analyses, N.K., N.F.J., W.D., A.P., M.P., and P.A.Z. analyzed the data; and N.K., M.P., and P.A.Z. wrote the article with aid of all authors.

Supplementary data

Supplementary data is available at NAR online.

Conflict of interest

None declared.

Funding

This work was supported by the National Science Center, Poland (NCN) grants 2020/39/I/NZ2/02464 to P.A.Z. and 2019/35/N/NZ2/02933 to N.K. M.P. acknowledges the support of the Ministry of Science and Innovation of Spain (PID2020-118038GB-I00/AEI/10.13039/501100011033) and European Union (TED2021-131852B-I00/AEI/10.13039/501100011033/Unión Europea NextGeneration EU/PRTR). Funding to pay the Open Access publication charges for this article was provided by Initiative of Excellence–Research University at Adam Mickiewicz University, Poznan, Poland.

Data availability

The data supporting this article can be accessed in the published version or its supplementary files. Additionally, raw genome sequencing data for the mutant *mlh1* and *bei10/+* Col \times *Ler* F₂ populations are deposited in the NCBI Sequence Read Archive (SRA) under the BioProject accession code PRJNA1156934.

This paper is linked to: doi:10.1093/nar/gkaf157.

References

- Villeneuve AM, Hillers KJ. Whence meiosis? *Cell* 2001;106:647–50. [https://doi.org/10.1016/S0092-8674\(01\)00500-1](https://doi.org/10.1016/S0092-8674(01)00500-1)
- McDonald MJ, Rice DP, Desai MM. Sex speeds adaptation by altering the dynamics of molecular evolution. *Nature* 2016;531:233–6. <https://doi.org/10.1038/nature17143>
- Mercier R, Mézard C, Jenczewski E *et al.* The molecular biology of meiosis in plants. *Annu Rev Plant Biol* 2015;66:297–327. <https://doi.org/10.1146/annurev-arplant-050213-035923>
- Wang Y, Copenhaver GP. Meiotic recombination: mixing it up in plants. *Annu Rev Plant Biol* 2018;69:577–609. <https://doi.org/10.1146/annurev-arplant-042817-040431>
- Lloyd A. Crossover patterning in plants. *Plant Reprod* 2023;36:55–72. <https://doi.org/10.1007/s00497-022-00445-4>
- Hunter N. Meiotic recombination: the essence of heredity. *Cold Spring Harb Perspect Biol* 2015;7:55–72. <https://doi.org/10.1101/cshperspect.a016618>
- Pyatnitskaya A, Borde V, De Muyt A. Crossing and zipping: molecular duties of the ZMM proteins in meiosis. *Chromosoma* 2019;128:181–98. <https://doi.org/10.1007/s00412-019-00714-8>
- Mercier R, Jolivet S, Vezon D *et al.* Two meiotic crossover classes cohabit in *Arabidopsis*: one is dependent on *MER3*, whereas the other one is not. *Curr Biol* 2005;15:692–701. <https://doi.org/10.1016/j.cub.2005.02.056>
- Higgins JD, Buckling EF, Franklin FCH *et al.* Expression and functional analysis of *AtMUS81* in *Arabidopsis* meiosis reveals a role in the second pathway of crossing-over. *Plant J* 2008;54:152–62. <https://doi.org/10.1111/j.1365-313X.2008.03403.x>
- Chelysheva L, Gendrot G, Vezon D *et al.* *Zip4/Spo22* is required for class I CO formation but not for synapsis completion in *Arabidopsis thaliana*. *PLoS Genet* 2007;3:e83. <https://doi.org/10.1371/journal.pgen.0030083>
- Berchowitz LE, Francis KE, Bey AL *et al.* The role of *AtMUS81* in interference-insensitive crossovers in *A. thaliana*. *PLoS Genet* 2007;3:e132. <https://doi.org/10.1371/journal.pgen.0030132>
- Higgins JD, Armstrong SJ, Franklin FCH *et al.* The *Arabidopsis* MutS homolog *AtMSH4* functions at an early step in recombination: evidence for two classes of recombination in

- Arabidopsis*. *Genes Dev* 2004;18:2557–70. <https://doi.org/10.1101/gad.317504>
13. Berchowitz LE, Copenhaver GP. Genetic interference: don't stand so close to me. *Curr Genomics* 2010;11:91–102. <https://doi.org/10.2174/138920210790886835>
 14. Girard C, Zwicker D, Mercier R. The regulation of meiotic crossover distribution: a coarse resolution to a century-old mystery? *Biochem Soc Trans* 2023;51:1179–90. <https://doi.org/10.1042/BST20221329>
 15. France MG, Enderle J, Röhrig S *et al*. ZYP1 is required for obligate cross-over formation and cross-over interference in *Arabidopsis*. *Proc Natl Acad Sci USA* 2021;118:e2021671118. <https://doi.org/10.1073/pnas.2021671118>
 16. Capilla-Pérez L, Durand S, Hurel A *et al*. The synaptonemal complex imposes crossover interference and heterochiasmy in *Arabidopsis*. *Proc Natl Acad Sci USA* 2021;118:e2023613118. <https://doi.org/10.1073/pnas.2023613118>
 17. Ziolkowski PA, Underwood CJ, Lambing C *et al*. Natural variation and dosage of the HEI10 meiotic E3 ligase control *Arabidopsis* crossover recombination. *Genes Dev* 2017;31:306–17. <https://doi.org/10.1101/gad.295501.116>
 18. Morgan C, Fozard JA, Hartley M *et al*. Diffusion-mediated HEI10 coarsening can explain meiotic crossover positioning in *Arabidopsis*. *Nat Commun* 2021;12:4674. <https://doi.org/10.1038/s41467-021-24827-w>
 19. Lian Q, Jing J, Ernst M *et al*. Joint control of meiotic crossover patterning by the synaptonemal complex and HEI10 dosage. *Nat Commun* 2022;13:5999. <https://doi.org/10.1038/s41467-022-33472-w>
 20. Morgan C, Howard M, Henderson IR. HEI10 coarsening, chromatin and sequence polymorphism shape the plant meiotic recombination landscape. *Curr Opin Plant Biol* 2024;81:102570. <https://doi.org/10.1016/j.pbi.2024.102570>
 21. Baker SM, Plug AW, Prolla TA *et al*. Involvement of mouse Mlh1 in DNA mismatch repair and meiotic crossing over. *Nat Genet* 1996;13:336–42. <https://doi.org/10.1038/ng0796-336>
 22. Wang TF, Kleckner N, Hunter N. Functional specificity of MutL homologs in yeast: evidence for three Mlh1-based heterocomplexes with distinct roles during meiosis in recombination and mismatch correction. *Proc Natl Acad Sci USA* 1999;96:13914–9. <https://doi.org/10.1073/pnas.96.24.13914>
 23. Jackson N, Sanchez-Moran E, Buckling E *et al*. Reduced meiotic crossovers and delayed prophase I progression in AtMLH3-deficient *Arabidopsis*. *EMBO J* 2006;25:1315–23. <https://doi.org/10.1038/sj.emboj.7600992>
 24. Argueso JL, Wanat J, Gemici Z *et al*. Competing crossover pathways act during meiosis in *Saccharomyces cerevisiae*. *Genetics* 2004;168:1805–16. <https://doi.org/10.1534/genetics.104.032912>
 25. Allers T, Lichten M. Differential timing and control of noncrossover and crossover recombination during meiosis. 2001;106:47–57.
 26. Marsolier-Kergoat M-C, Khan MM, Schott J *et al*. Mechanistic view and genetic control of DNA recombination during meiosis. *Mol Cell* 2018;70:9–20. <https://doi.org/10.1016/j.molcel.2018.02.032>
 27. Zakharyevich K, Tang S, Ma Y *et al*. Delineation of joint molecule resolution pathways in meiosis identifies a crossover-specific resolvase. *Cell* 2012;149:334–47. <https://doi.org/10.1016/j.cell.2012.03.023>
 28. Cannavo E, Sanchez A, Anand R *et al*. Regulation of the MLH1–MLH3 endonuclease in meiosis. *Nature* 2020;586:618–22. <https://doi.org/10.1101/2020.02.12.946293>
 29. Kulkarni D, Owens S, Honda M *et al*. PCNA activates the MutLγ endonuclease to promote meiotic crossing over. *Nature* 2020;586:623–7. <https://doi.org/10.1038/s41586-020-2645-6>
 30. Claeys Bouuaert C, Keeney S. Distinct DNA-binding surfaces in the ATPase and linker domains of MutLγ determine its substrate specificities and exert separable functions in meiotic recombination and mismatch repair. *PLoS Genet* 2017;13:e1006722. <https://doi.org/10.1371/journal.pgen.1006722>
 31. Barlow AL, Hultén MA. Crossing over analysis at pachytene in man. *Eur J Hum Genet* 1998;6:350–8. <https://doi.org/10.1038/sj.ejhg.5200200>
 32. Anderson LK, Reeves A, Webb LM *et al*. Distribution of crossing over on mouse synaptonemal complexes using immunofluorescent localization of MLH1 protein. *Genetics* 1999;151:1569–79. <https://doi.org/10.1093/genetics/151.4.1569>
 33. Dion E, Li L, Jean M *et al*. An *Arabidopsis* MLH1 mutant exhibits reproductive defects and reveals a dual role for this gene in mitotic recombination. *Plant J* 2007;51:431–40. <https://doi.org/10.1111/j.1365-313X.2007.03145.x>
 34. Alou AH, Jean M, Domingue O *et al*. Structure and expression of AtPMS1, the *Arabidopsis* ortholog of the yeast DNA repair gene PMS1. *Plant Sci* 2004;167:447–56. <https://doi.org/10.1016/j.plantsci.2004.04.012>
 35. Li L, Dion E, Richard G *et al*. The *Arabidopsis* DNA mismatch repair gene PMS1 restricts somatic recombination between homeologous sequences. *Plant Mol Biol* 2009;69:675–84. <https://doi.org/10.1007/s11103-008-9447-9>
 36. Kurzbauer MT, Pradillo M, Kerzendorfer C *et al*. *Arabidopsis thaliana* FANCD2 promotes meiotic crossover formation. *Plant Cell* 2018;30:415–28. <https://doi.org/10.1105/tpc.17.00745>
 37. Li X, Zhang J, Huang J *et al*. Regulation of interference-sensitive crossover distribution ensures crossover assurance in *Arabidopsis*. *Proc Natl Acad Sci USA* 2021;118:e2107543118. <https://doi.org/10.1073/pnas.2107543118>
 38. Hartung F, Suer S, Puchta H. Two closely related RecQ helicases have antagonistic roles in homologous recombination and DNA repair in *Arabidopsis thaliana*. *Proc Natl Acad Sci USA* 2007;104:18836–41. <https://doi.org/10.1073/pnas.0705998104>
 39. Girard C, Chelysheva L, Choinard S *et al*. AAA-ATPase FIDGETIN-LIKE 1 and helicase FANCM antagonize meiotic crossovers by distinct mechanisms. *PLoS Genet* 2015;11:e1005369. <https://doi.org/10.1371/journal.pgen.1005369>
 40. Séguéla-Arnaud M, Crismani W, Larchevêque C *et al*. Multiple mechanisms limit meiotic crossovers: TOP3α and two BLM homologs antagonize crossovers in parallel to FANCM. *Proc Natl Acad Sci USA* 2015;112:4713–8. <https://doi.org/10.1073/pnas.1423107112>
 41. Crismani W, Girard C, Froger N *et al*. FANCM limits meiotic crossovers. *Science* 2012;336:1588–90. <https://doi.org/10.1126/science.1220381>
 42. Melamed-Bessudo C, Yehuda E, Stuitje AR *et al*. A new seed-based assay for meiotic recombination in *Arabidopsis thaliana*. *Plant J* 2005;43:458–66. <https://doi.org/10.1111/j.1365-313X.2005.02466.x>
 43. Hord CLH, Sun YJ, Pillitteri LJ *et al*. Regulation of *Arabidopsis* early anther development by the mitogen-activated protein kinases, MPK3 and MPK6, and the ERECTA and related receptor-like kinases. *Mol Plant* 2008;1:645–58. <https://doi.org/10.1093/mp/ssn029>
 44. Alexander MP. Differential staining of aborted and nonaborted pollen. *Biotech Histochem* 1969;44:117–22.
 45. Wu G, Rossidivito G, Hu T *et al*. Traffic lines: new tools for genetic analysis in *Arabidopsis thaliana*. *Genetics* 2015;200:35–45. <https://doi.org/10.1534/genetics.114.173435>
 46. Kbiri N, Dluzewska J, Henderson IR *et al*. Quantifying meiotic crossover recombination in *Arabidopsis* lines expressing fluorescent reporters in seeds using SeedScoring pipeline for CellProfiler. In: *Methods in Molecular Biology*. Vol: 2484. New York, NY: Humana, 2022, 121–34. https://doi.org/10.1007/978-1-0716-2253-7_10
 47. Martinez-Garcia M, Pradillo M. Functional analysis of *Arabidopsis* argonauts in meiosis and DNA repair. In: *Methods in Molecular Biology*. Vol: 1640. New York, NY: Humana Press, 2017, 145–58. https://doi.org/10.1007/978-1-4939-7165-7_10

48. Zhu L, Fernández-Jiménez N, Szymanska-Lejman M *et al.* Natural variation identifies SNI1, the SMC5/6 component, as a modifier of meiotic crossover in *Arabidopsis*. *Proc Natl Acad Sci USA* 2021;118:e2021970118. <https://doi.org/10.1073/pnas.2021970118>
49. Sanchez Moran E, Armstrong SJ, Santos JL *et al.* Chiasma formation in *Arabidopsis thaliana* accession Wassileskija and in two meiotic mutants. *Chromosome Res* 2001;9:121–8. <https://doi.org/10.1023/A:1009278902994>
50. Ross KJ, Franz P, Jones GH. A light microscopic atlas of meiosis in *Arabidopsis thaliana*. *Chromosome Res* 1996;4:507–16. <https://doi.org/10.1007/BF02261778>
51. Campell BR, Song Y, Posch TE *et al.* Sequence and organization of 5S ribosomal RNA-encoding genes of *Arabidopsis thaliana*. *Gene* 1992;112:225–8. [https://doi.org/10.1016/0378-1119\(92\)90380-8](https://doi.org/10.1016/0378-1119(92)90380-8)
52. Bieluszewski T, Szymanska-Lejman M, Dziegielewski W *et al.* Efficient generation of CRISPR/Cas9-based mutants supported by fluorescent seed selection in different *Arabidopsis* accessions. In: *Methods in Molecular Biology*. Vol: 2484. New York, NY: Humana, 2022, 161–82. https://doi.org/10.1007/978-1-0716-2253-7_13
53. Rowan BA, Patel V, Weigel D *et al.* Rapid and inexpensive whole-genome genotyping-by-sequencing for crossover localization and fine-scale genetic mapping. *G3: Genes/Genomes/Genetics* 2015;5:385–98. <https://doi.org/10.1534/g3.114.016501>
54. Szymanska-Lejman M, Dziegielewski W, Dlużewska J *et al.* The effect of DNA polymorphisms and natural variation on crossover hotspot activity in *Arabidopsis* hybrids. *Nat Commun* 2023;14:33. <https://doi.org/10.1038/s41467-022-35722-3>
55. Dlużewska J, Dziegielewski W, Szymanska-Lejman M *et al.* MSH2 stimulates interfering and inhibits non-interfering crossovers in response to genetic polymorphism. *Nat Commun* 2023;14:6716. <https://doi.org/10.1038/s41467-023-42511-z>
56. Langmead B, Salzberg SL. Fast gapped-read alignment with Bowtie 2. *Nat Methods* 2012;9:357–9. <https://doi.org/10.1038/nmeth.1923>
57. Li H, Handsaker B, Wysoker A *et al.* The sequence alignment/map format and SAMtools. *Bioinformatics* 2009;25:2078–9. <https://doi.org/10.1093/bioinformatics/btp352>
58. Li H. A statistical framework for SNP calling, mutation discovery, association mapping and population genetical parameter estimation from sequencing data. *Bioinformatics* 2011;27:2987–93. <https://doi.org/10.1093/bioinformatics/btr509>
59. Rowan BA, Heavens D, Feuerborn TR *et al.* An ultra high-density *Arabidopsis thaliana* crossover. *Genetics* 2019;213:771–87. <https://doi.org/10.1534/genetics.119.302406>
60. Langmead B, Salzberg SL. Fast gapped-read alignment with Bowtie 2. *Nat Methods* 2012;9:357–9. <https://doi.org/10.1038/nmeth.1923>
61. Li H, Durbin R. Fast and accurate short read alignment with Burrows–Wheeler transform. *Bioinformatics* 2009;25:1754–60. <https://doi.org/10.1093/bioinformatics/btp324>
62. Pedersen BS, Quinlan AR. Mosdepth: quick coverage calculation for genomes and exomes. *Bioinformatics* 2018;34:867–8. <https://doi.org/10.1093/bioinformatics/btx699>
63. White MA, Wang S, Zhang L *et al.* Quantitative modeling and automated analysis of meiotic recombination. *Methods Mol Biol* 2017;1471:305–23. https://doi.org/10.1007/978-1-4939-6340-9_18
64. Ziolkowski PA. Why do plants need the ZMM crossover pathway? A snapshot of meiotic recombination from the perspective of interhomolog polymorphism. *Plant Reprod* 2022;1:3.
65. Henry IM, Dilkes BP, Miller ES *et al.* Phenotypic consequences of aneuploidy in *Arabidopsis thaliana*. *Genetics* 2010;186:1231–45. <https://doi.org/10.1534/genetics.110.121079>
66. Hintzen DC, Soto M, Schubert M *et al.* The impact of monosomies, trisomies and segmental aneuploidies on chromosomal stability. *PLoS One* 2022;17:e0268579. <https://doi.org/10.1371/journal.pone.0268579>
67. Zhao Z-Y, Weber DF. Male gametophyte development in monosomics of maize. *Genome* 1989;32:155–64. <https://doi.org/10.1139/g89-423>
68. Franz PF, Armstrong S, de Jong JH *et al.* Integrated cytogenetic map of chromosome arm 4S of *A. thaliana*: structural organization of heterochromatic knob and centromere region. *Cell* 2000;100:367–76. [https://doi.org/10.1016/S0092-8674\(00\)80672-8](https://doi.org/10.1016/S0092-8674(00)80672-8)
69. Zapata L, Ding J, Willing E-M *et al.* Chromosome-level assembly of *Arabidopsis thaliana* L *er* reveals the extent of translocation and inversion polymorphisms. *Proc Natl Acad Sci USA* 2016;113:E4052–60. <https://doi.org/10.1073/pnas.1607532113>
70. Serra H, Lambing C, Griffin CH *et al.* Massive crossover elevation via combination of HEI10 and recq4a recq4b during *Arabidopsis* meiosis. *Proc Natl Acad Sci USA* 2018;115:2437–42. <https://doi.org/10.1073/pnas.1713071115>
71. Blackwell AR, Dlużewska J, Szymanska-Lejman M *et al.* MSH2 shapes the meiotic crossover landscape in relation to interhomolog polymorphism in *Arabidopsis*. *EMBO J* 2020;39:e104858. <https://doi.org/10.15252/emj.2020104858>
72. Drouaud J, Camilleri C, Bourguignon P *et al.* Variation in crossing-over rates across chromosome 4 of *Arabidopsis thaliana* reveals the presence of meiotic recombination “hot spots”. *Genome Res* 2006;16:106–14. <https://doi.org/10.1101/gr.4319006>
73. Sun H, Rowan BA, Flood PJ *et al.* Linked-read sequencing of gametes allows efficient genome-wide analysis of meiotic recombination. *Nat Commun* 2019;10:4310. <https://doi.org/10.1038/s41467-019-12209-2>
74. Knoll A, Higgins JD, Seeliger K *et al.* The Fanconi anemia ortholog FANCM ensures ordered homologous recombination in both somatic and meiotic cells in *Arabidopsis*. *Plant Cell* 2012;24:1448–64. <https://doi.org/10.1105/tpc.112.096644>
75. Bishop DK, Park D, Xu L *et al.* DMC1: a meiosis-specific yeast homolog of *E. coli* recA required for recombination, synaptonemal complex formation, and cell cycle progression. *Cell* 1992;69:439–56. [https://doi.org/10.1016/0092-8674\(92\)90446-J](https://doi.org/10.1016/0092-8674(92)90446-J)
76. Kurzbauer M, Uanschou C, Chen D *et al.* The recombinases DMC1 and RAD51 are functionally and spatially separated during meiosis in *Arabidopsis*. *Plant Cell* 2012;24:2058–70. <https://doi.org/10.1105/tpc.112.098459>
77. Al-Sweel N, Raghavan V, Dutta A *et al.* mlh3 mutations in baker’s yeast alter meiotic recombination outcomes by increasing noncrossover events genome-wide. *PLoS Genet* 2017;13:55–72. <https://doi.org/10.1371/journal.pgen.1006974>
78. Pyatnitskaya A, Andreani J, Guérois R *et al.* The Zip4 protein directly couples meiotic crossover formation to synaptonemal complex assembly. *Genes Dev* 2022;36:53–69. <https://doi.org/10.1101/gad.348973.121>
79. Zhang Q, Ji SY, Busayavalasa K *et al.* SPO16 binds SHOC1 to promote homologous recombination and crossing-over in meiotic prophase I. *Sci Adv* 2019;5:eaa9780.
80. Toledo M, Sun X, Briño-Enríquez MA *et al.* A mutation in the endonuclease domain of mouse MLH3 reveals novel roles for mutly during crossover formation in meiotic prophase I. *PLoS Genet* 2019;15:e1008177. <https://doi.org/10.1371/journal.pgen.1008177>
81. Lipkin SM, Moens PB, Wang V *et al.* Meiotic arrest and aneuploidy in MLH3-deficient mice. *Nat Genet* 2002;31:385–90. <https://doi.org/10.1038/ng931>
82. Osman K, Sanchez-Moran E, Mann SC *et al.* Replication protein A (AtRPA1a) is required for class I crossover formation but is dispensable for meiotic DNA break repair. *EMBO J* 2009;28:394–404. <https://doi.org/10.1038/emboj.2008.295>
83. Chelysheva L, Vezon D, Chambon A *et al.* The *Arabidopsis* HEI10 is a new ZMM protein related to Zip3. *PLoS Genet* 2012;8:e1002799. <https://doi.org/10.1371/journal.pgen.1002799>

84. Blary A, Gonzalo A, Eber F *et al.* FANCM limits meiotic crossovers in *Brassica* crops. *Front Plant Sci* 2018;368:9.
85. Desjardins SD, Simmonds J, Guterman I *et al.* FANCM promotes class I interfering crossovers and suppresses class II non-interfering crossovers in wheat meiosis. *Nat Commun* 2022;13:3644. <https://doi.org/10.1038/s41467-022-31438-6>
86. Mieulet D, Aubert G, Bres C *et al.* Unleashing meiotic crossovers in crops. *Nature Plants* 2018;4:1010–16. <https://doi.org/10.1038/s41477-018-0311-x>
87. De Muyt A, Jessop L, Kolar E *et al.* BLM helicase ortholog Sgs1 is a central regulator of meiotic recombination intermediate metabolism. *Mol Cell* 2012;46:43–53. <https://doi.org/10.1016/j.molcel.2012.02.020>
88. Pannafino G, Chen JJ, Mithani V *et al.* The Dmc1 recombinase physically interacts with and promotes the meiotic crossover functions of the Mlh1–Mlh3 endonuclease. *Genetics* 2024;227:iyae066. <https://doi.org/10.1093/genetics/iyae066>